ENHANCING QED EFFECTS BY TEMPORAL PULSE SHAPING IN LASER - ELECTRON-BEAM COLLISIONS

LAURENCE E. BRADLEY

Master of Science by Research

University of York

Physics

June 2019

ABSTRACT

Quantum stochastic radiation reaction and electron-positron pair production influence the dynamics of plasmas created by laser pulses with high-intensity $\geq 10^{23}\mathrm{Wcm}^{-2}$. Experimental evidence of quantum effects has proven challenging to obtain so far and crucially depend on maximising the electron's Lorentz invariant non-linearity parameter, $\chi_e = E_{\mathrm{RF}}/E_{\mathrm{crit}}$, the ratio of the laser electric field observed by the electron in its rest frame E_{RF} to the critical field E_{crit} of quantum electrodynamics (QED).

By deriving the average χ_e ab initio, we find the initial electron energy is crucial as radiation reaction discourages maximum χ_e before the electrons reach the peak intensity. In the following, we use a QED-PIC code to simulate the collision of a counter-propagating $5 \times 10^{21}\mathrm{Wcm}^{-2}$ laser pulse with a 1.5GeV electron-beam. Simulating both symmetric and skewed Gaussian pulses, where the leading edge of the temporal intensity envelope has a fast rise time, leads to an undesirable reduction to the peak intensity I_0.

Contrary to the widely accepted result, we show that the optimum temporal envelope to enhance pair production is a short and compressed Gaussian pulse. A skewed Gaussian results in approximately 1.5×10^{-6} pairs produced per electron and is enhanced by a factor of ~ 10 to an improvement of 2.0×10^{-5}. To this end, we consider an alternative approach using plasma optics to reach maximum χ_e to enhance electron-positron pair production.

CONTENTS

LIST OF FIGURES

ACKNOWLEDGMENTS

Acknowledgment is given to my supervisor Dr. Chris Ridgers for many interesting discussions, support and encouragement to pursue this compelling field of research. Temporal envelope data has kindly been provided by M. J. V. Streeter at Blackett Laboratory, Imperial College London, London SW7 2AZ, UK. Computing resources provided by the York Plasma Institute and STFC Scientific Computing Department's SCARF cluster.

DECLARATION

I declare that this thesis is a presentation of original work and I am the sole author. This work has not previously been presented for an award at this, or any other, University. All sources are acknowledged as References.

Laurence E. Bradley

Publications

L.E. Bradley, et al "Optimal temporal pulse shape to enhance QED effects in laser - electron-beam collisions", New. J. Phys. (in preparation)

1

INTRODUCTION

1.1 MOTIVATION

Near-future multi-PW laser facilities such as Vulcan 20PW [1], Extreme Light Infrastructure [2] and Apollon [3] are expected to reach focused intensities of $\geq 10^{23}\text{Wcm}^{-2}$. Reaching this intensity will enable us to explore new plasma physics in the relativistic regime in which strong-field quantum electrodynamics (QED) can significantly alter the dynamics of a plasma [4]. One important dominant effect at play is the radiation reaction (RR) effect due to the conservation of energy as charged particles in a strong laser field emit electromagnetic radiation. The effect of RR can lead to nearly complete absorption of the laser pulse in the classical picture [5]. Deepening our understanding of the transition between classical and quantum radiation reaction has been at the forefront of theoretical research [6, 7, 8] with recent experimental progress [9, 10, 11].

Experimental techniques such as chirped-pulse amplification (CPA) have enabled ultrashort lasers with femtosecond (fs) durations [12, 13] to become a reality [14]. A feature of the development of high-intensity lasers has been the rapid increase in laser intensity as new generation facilities come online, as illustrated in fig 1.1 [15]. Current laser systems have reached a record peak intensity of $I_0 \sim 0.7 \times 10^{22}\text{Wcm}^{-2}$ [16], an order of magnitude less than the intensity expected at the next generation laser facilities.

Experiments at these facilities will be investigating plasmas in the highly non-linear regime, in which the particles exhibit stochastic effects. One such effect is quantum stochastic RR, where the emission of highly energetic photons is discrete and unpredictable. If the hard photons reach an energy threshold then non-linear Breit-Wheeler (BW) pair processes can arise.

This process is the effect of an emitted high energy photon from the electrons that interact with the laser pulse photons, annihilate thus creating an electron-positron pair. If the electromagnetic field produced by the laser is strong enough, a pair cascade involving multiple pairs can be initiated producing a so-called QED-plasma. The importance of quantum effects on the electron is measured by the Lorentz-invariant non-linearity parameter χ_e. It is determined by calculating the ratio of the electric field of the electron observed in its rest frame E_{RF} to the *critical* or *Schwinger* field [17] E_{crit}

$$\chi_e = \frac{E_{\mathrm{RF}}}{E_{\mathrm{crit}}} \tag{1.1}$$

where the value of E_{crit} is the strength of the electric field required to break down the vaccum into spontaneous electron-positron pairs and has a value

$$E_{\mathrm{crit}} = \frac{m_e^2 c^3}{q_e \hbar} \simeq 1.32 \times 10^{18} \mathrm{Vm}^{-1}$$

However, this electric field magnitude is unattainable with current and near-future laser systems. We may overcome this constraint by accelerating the electrons externally to an energy $\gamma \sim a_0$. The laser strength parameter a_0, or normalised vector potential a_0 is defined as the electron energy gained over a distance of the laser wavelength in units of its rest energy $m_e c^2$. The value of the electron's χ_e scales linearly with the strength parameter a_0 showing the dependence of laser intensity to

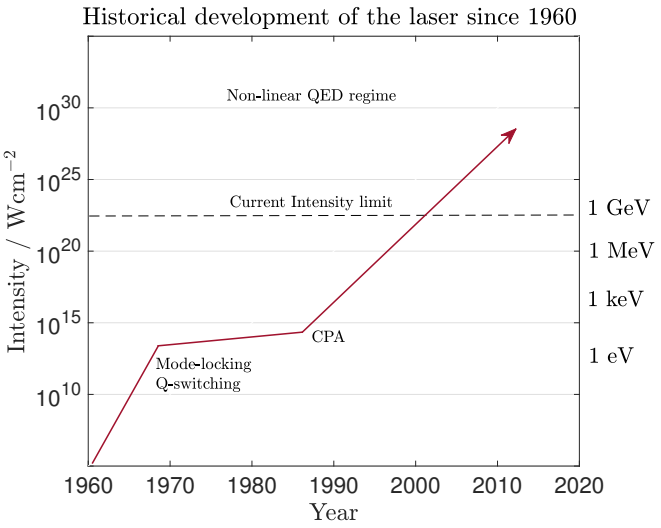

Figure 1.1: Rapid increase in laser intensity from 1960 to modern day.

observe quantum effects at ($\chi_e \geq 0.1$). A convenient approximation to the strength parameter a_0 is given by

$$a_0 \approx 0.85\sqrt{\frac{I\lambda^2}{10^{18}\mathrm{Wcm}^{-2}\mu\mathrm{m}^2}}$$

where λ is the laser wavelength. A laser with a wavelength 1μm and intensity $1 \times 10^{21}\mathrm{Wcm}^{-2}$ such that $a_0 \approx 27$ and since $a_0 \gg 1$ would produce electrons that are influenced by strong-field QED effects. Illustrated in fig. 1.2 shows how the magnitude of a_0 has increased over years with increasing laser intensities. We can find that multi-PW lasers such as Vulcan 20PW and the Extreme Light Infrastructure will be reaching in excess of $a_0 \sim 100$, in a regime that produces sufficiently strong electromagnetic fields to frequently observe quantum effects.

Bula *et al* [18] reports on the non-linear Compton scattering experiments performed at the SLAC facility. Using a 7ps laser with a moderate intensity of $1.3 \times 10^{18}\mathrm{Wcm}^{-2}$ ($a_0 = 0.5$) with a 46.6GeV beam, electrons colliding with a $\chi_e = 0.36$ were measured from the scattered electrons. In these experiments, highly energetic gamma rays were emitted reaching an energy high enough to decay into electron-positron

pairs. The experiment observed 101 real e^-e^+ pairs and 69 ± 14 for electrons with a value $\chi_e > 0.216$ [19]. The increases of the electron's χ_e only have to be small in order to have a significant effect on pair yields, showing the importance of maximising χ_e if we wish to observe pair cascades in the intense laser field.

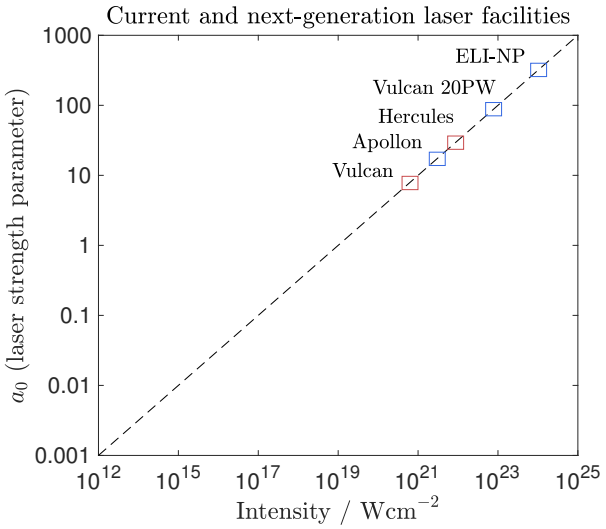

Figure 1.2: Laser strength parameter a_0 increasing proportionally with laser intensity reaching new limits. Shown in red are current laser systems while near-future facilities are indicated in blue.

The purpose of this thesis is to consider the dependency the temporal shape of the laser pulse has on maximising magnitudes of the electron's non-linearity parameter χ_e. Understanding the parameters and optimum temporal shape of the laser pulse to increase χ_e and therefore the electron-positron pair yields will be crucial in experiments performed at next generation laser facilities [20].

This research has applications to, most evidently, the creation of real laboratory electron-positron pairs [21] and quantum effects in extreme astronomical contexts [22]. The following will identify the experimental constraints of modifying the pulse and if pair enhancement is achieved with a laser pulse that propagates with an asymmetric temporal intensity envelope.

A variety of experimental schemes [23, 24] and simulation methods [25, 26, 27] to maximise electron-positron pair yields have previously been proposed. Asymmetric [28] and supergaussian envelopes [29] in particular have been suggested to encourage a variety of enhancements. Most notable of these are the Leemans experiments, employing both Gaussian and skewed Gaussian pulse shapes. Leemans *et al* [30] discovered that modifying the shape of a short 76fs laser pulse to an asymmetric temporal pulse enhanced the electron yield in a plasma wakefield. This is due to larger amplitude wakes forming at the fast rising leading edge of the pulse. These results were the first experimentally achieved enhancement using a non-linear laser chirp.

In this thesis, the collision of a counter-propagating circularly polarised laser - electron-beam is considered. Simulations using the particle-in-cell (PIC) code EPOCH-1D will be employed to produce symmetric, asymmetric and supergaussian temporal envelopes. We will further use realistic Gaussian temporal envelopes from optical phase offsetting and data from a Laser Wakefield Acceleration (LWFA) simulation in the Fourier-Bessel PIC (FBPIC) code [31]. The analytical forms for the evolution of the electron's average $\gamma(t)$ and $\chi_e(t)$ are derived *ab initio* and compared with results from PIC code simulations. A scheme that uses plasma optics will be proposed in order to suggest an effective method for producing pulses with a sharp fast rising edge at the front of the laser pulse.

1.1.1 *Notation & units*

Covariant relativistic four-momentum of a particle with mass m and Lorentz factor γ

$$p^\mu = (\gamma mc, p_i)$$

contravariant form of the four-momentum is

$$p^\mu = (\gamma mc, -p_i)$$

Four-gradient in covariant form

$$\partial_\mu = \left(\frac{1}{c}\frac{\partial}{\partial t}, \nabla\right)$$

and contravariant form

$$\partial^\mu = \left(\frac{1}{c}\frac{\partial}{\partial t}, -\nabla\right)$$

Covariant electromagnetic field tensor in component form

$$F_{\mu\nu} = \partial_\mu A_\nu - \partial_\nu A_\mu$$

where A is the four-potential $A^\alpha = (\phi/c, \mathbf{A})$, ϕ the electric potential.

The matrix form of the electromagnetic field tensor is

$$F_{\mu\nu} = \begin{pmatrix} 0 & E_x/c & E_y/c & E_z/c \\ -E_x/c & 0 & -B_z & B_y \\ -E_y/c & B_z & 0 & -B_x \\ -E_z/c & -B_y & B_x & 0 \end{pmatrix}$$

Contravariant electromagnetic field tensor

$$F^{\mu\nu} = \begin{pmatrix} 0 & -E_x/c & -E_y/c & -E_z/c \\ E_x/c & 0 & -B_z & B_y \\ E_y/c & B_z & 0 & -B_x \\ E_z/c & -B_y & B_x & 0 \end{pmatrix}$$

Name	Notation	Value	SI Units
Speed of light in vacuum	c	2.998×10^{8}	ms^{-1}
Electron mass	m_e	9.11×10^{-31}	kg
Charge of Electron	q_e	1.6×10^{-19}	C
Compton wavelength ($\hbar/mc$)	λ_c	2.426310×10^{-12}	m
Fine structure constant	a_0	7.30×10^{-3}	1
Critical field ($m_e c^3/q_e\hbar$)	E_s	1.32×10^{18}	Vm^{-1}
Vacuum permittivity	ϵ_0	8.85×10^{-12}	Fm^{-1}
Reduced Plank constant	$\hbar$	1.06×10^{-34}	Js^{-1}
Compton time (λ_c/c)	τ_c	1.29×10^{-21}	s

Table 1.1: Definition of fundamental constants

1.2 CLASSICAL ELECTRODYNAMICS

1.2.1 *Forces on charged particles*

The Abraham-Lorentz force is the effect of a charged particle emitting electromagnetic radiation as the particle with charge q accelerates. It is a recoil force that occurs under the assumption that the velocity of the particle is much less than the speed of light c. It can be derived simply by following [32], consider the work done on the particle, which is equal to integrating the negative Larmor power, where $P \propto q^2\mathbf{a}^2$ [33] between periodic times t_1 and t_2

$$\int_{t_1}^{t_2} \mathbf{F}\cdot\mathbf{v}\ dt = \int_{t_1}^{t_2} -P\ dt = -\int_{t_1}^{t_2} \frac{\mu_0 q^2}{6\pi c}\mathbf{a}^2\ dt = -\frac{\mu_0 q^2}{6\pi c}\int_{t_1}^{t_2} \dot{\mathbf{v}}\cdot\dot{\mathbf{v}}\ dt$$

Using the method of integration by parts

$$\int_{t_1}^{t_2} \mathbf{F} \cdot \mathbf{v}\ dt = -\frac{\mu q^2}{6\pi c}\dot{\mathbf{v}} \cdot \mathbf{v}\Big|_{t_1}^{t_2} + \frac{\mu_0 q^2}{6\pi c}\int_{t_1}^{t_2} \ddot{\mathbf{v}} \cdot \mathbf{v}\ dt$$
$$= \frac{\mu_0 q^2}{6\pi c}\int_{t_1}^{t_2} \dot{\mathbf{a}} \cdot \mathbf{v}\ dt$$

comparing the integrands, the damping force on the particle is

$$\mathbf{F} = \frac{\mu_0 q^2}{6\pi c}\dot{\mathbf{a}}$$

where μ_0 is the permittivity of free space. This result is the most fundamental form of radiation reaction. This equation suggests that the force on a particle is proportional to the square of its charge and the derivative of the particles acceleration. From Newton's second law $|\mathbf{F}| = m|\mathbf{a}|$

$$F = \frac{\mu_0 q^2}{6\pi c}\dot{a} = ma$$

We can see the solution to the acceleration has an exponential form, namely $a(t) = a_0 e^{t/\tau}$. A solution of this type is called a *runaway* solution since it produces unphysical results in which the particles acceleration exponentially increases. This seemingly unavoidable solution has been fixed with the self-consistent Landau-Lifshitz equation, taking into account the classical recoil from radiation and has been solved exactly for a plane electromagnetic wave [34, 35].

1.2.2 *Generalised Lorentz force on a particle*

A particle with charge q and velocity $\mathbf{v}$ will experience a force in the presence of an external electric $\mathbf{E}$ and magnetic field $\mathbf{B}$. This is the

Lorentz force and acts perpendicular to $\mathbf{E} \times \mathbf{B}$, in tensorial form the Lorentz force law reads

$$\frac{dp^{\mu}}{d\tau} = qF^{\mu\nu}U_{\nu} \tag{1.2}$$

where $p^{\mu} = (\gamma mc, p_i)$ is the four-momentum, q is the charge of the particle, $U_{\nu} = \gamma(c, -v_i)$ is its four-velocity and $F^{\mu\nu}$ is the rank-2 anti-symmetric electromagnetic field tensor

$$F^{\mu\nu} = \begin{pmatrix} 0 & -E_x/c & -E_y/c & -E_z/c \\ E_x/c & 0 & -B_z & B_y \\ E_y/c & B_z & 0 & -B_x \\ E_z/c & -B_y & B_x & 0 \end{pmatrix}$$

The vector form of eqn 1.2 can be derived simply by considering the force in the x-direction as follows

$$\frac{dp^1}{d\tau} = qF^{1\nu}U_{\nu} = q(U_0F^{10} + U_1F^{11} + U_2F^{12} + U_3F^{13})$$

Substituting the elements of $F^{\mu\nu}$

$$\frac{dp^1}{d\tau} = q\left(U_0\left(\frac{E_x}{c}\right) + U_1(0) + U_2(-B_z) + U_3(B_y)\right)$$

Now substituting the components of the four-velocity noticing the factor γ that appears yields

$$\begin{aligned} \frac{dp^1}{d\tau} &= q\gamma\left(c\left(\frac{E_x}{c}\right) + (-v_x)(0) + (-v_y)(-B_z) + (-v_z)(B_y)\right) \\ &= q\gamma(E_x + v_xB_z - v_zB_y) \\ &= q\gamma(E_x + \mathbf{v} \times \mathbf{B}_x) \end{aligned}$$

Identical procedure can be performed in both the yz-directions respectively to give

$$\frac{d\mathbf{P}}{d\tau} = q\gamma(\mathbf{E} + \mathbf{v} \times \mathbf{B})$$

where $\mathbf{P}$ is the relativistic momentum $\mathbf{P} = \gamma m\mathbf{v}$. The particles proper time $d\tau$ is related to coordinate time dt via the inverse Lorentz factor γ where $d\tau = dt/\gamma$. The relativistic Lorentz force law in coordinate time then becomes

$$\frac{d\mathbf{P}}{dt} = q(\mathbf{E} + \mathbf{v} \times \mathbf{B})$$

Arriving at the familiar result of the Lorentz force on a particle with charge q, electric field $\mathbf{E}$ and magnetic field $\mathbf{B}$, namely

$$\mathbf{F} = q(\mathbf{E} + \mathbf{v} \times \mathbf{B})$$

The radiation reaction force on an electron is negligible in weak fields but becomes comparable to the Lorentz force as γE_L approaches E_{crit}, the critical electric field strength of quantum electrodynamics. We shall see radiation reaction is highly dependent on the laser field E_L amongst other parameters such as the initial energy of the electrons.

1.2.3 *Non-linear Compton Scattering*

Synchrotron radiation or non-linear Compton scattering for $a_0 \gg 1$ is the effect of photon emission as the charge is accelerated in an electromagnetic field. However, if the magnetic field is static, the radiation is described as magnetic bremstrahlung [36]. The synchrotron emission below is described for $a_0 \gg 1$ and the laser field in the lab frame $E_L \ll E_{\text{crit}}$

The emission process of an electron $e^-(p, \chi_e)$ with momentum p and non-linearity parameter χ_e emits a gamma-ray hard photon $\gamma(k, \chi_\gamma)$ with a wave vector k and photon non-linearity parameter χ_γ, which is

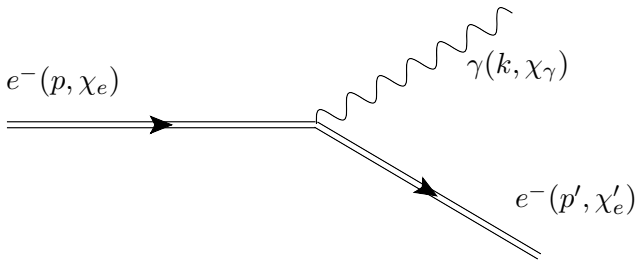

Figure 1.3: A dressed state electron $e^-(p, \chi_e)$ with momentum p and non-linearity parameter χ_e emits a gamma-ray photon $\gamma(k, \chi_\gamma)$ with wave vector k and analogous photon parameter χ_γ. After the emission, the electron recoils and changing in motion, loosing momentum to p' and a reduced χ'_e to $e^-(p', \chi'_e)$.

analogous to χ_e but for a photon. As the photon is emitted, a fraction of the electron's energy is lost and from the conservation of energy the electron changes its motion to a new reduced energy and momentum state $e^-(p', \chi'_e)$. The rate of gamma-ray photon emission is determined by the rate of emission equation following V. N. Baier *et al* [37]

$$\frac{d^2 N_\gamma}{d\chi_\gamma dt} = \frac{\sqrt{3}\alpha_f c}{\lambda_c} \frac{cB}{E_{\text{crit}}} \frac{F(\chi_e, \chi_\gamma)}{\chi_\gamma} \tag{1.3}$$

where α_f is the fine structure constant, $\lambda_c = 2.4263 \times 10^{-12}\text{m}$ is the Compton wavelength, B is the magnitude of the magnetic field. Now allowing $\chi_e = \gamma cB/E_{\text{crit}}$ from $|\mathbf{E}| = c|\mathbf{B}|$, multiplying by the electron's γ and integrating over the photon non-linearity parameter χ_γ

$$\int \gamma \frac{d^2 N_\gamma}{d\chi_\gamma dt} d\chi_\gamma = \int \frac{\sqrt{3}\alpha_f c}{\lambda_c} \frac{\chi_e}{\gamma} \gamma \frac{F(\chi_e, \chi_\gamma)}{\chi_\gamma} d\chi_\gamma$$

$$\gamma \frac{dN_\gamma}{dt} = \frac{\sqrt{3}\alpha_f c}{\lambda_c} \chi_e \int \frac{F(\chi_e, \chi_\gamma)}{\chi_\gamma} d\chi_\gamma$$

thus

$$\frac{dN_\gamma}{dt} = \frac{\sqrt{3}\alpha_f c}{\lambda_c} \frac{\chi_e}{\gamma} h(\chi_e) = \lambda_\gamma(\chi_e) \tag{1.4}$$

is the photon emission rate parameterised by χ_e, where $h(\chi_e)$ is an integral over the synchrotron function $F(\chi_e, \chi_\gamma)$

$$h(\chi_e) = \int_0^{\chi_e/2} \frac{F(\chi_e, \chi_\gamma)}{\chi_\gamma} d\chi_\gamma$$

where Baier *et al* [37] gives the following lower and upper χ_e limits

$$h(\chi_e) = \begin{cases} 5.236(1 - 0.345\chi_e + 3.5\chi_e^2) & \chi_e \ll 1, \\ 5.298\chi_e^{-0.333} & \chi_e \gg 1 \end{cases} \tag{1.5}$$

We can show the rate of photon synchrotron emission by electron's at $\chi_e \geq 1$ which is plotted in fig 1.4.

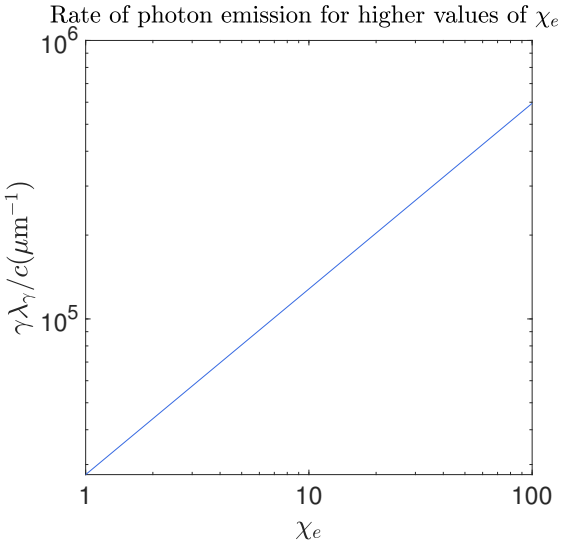

Figure 1.4: Rate of photon emission given in eqn 1.4 for electrons with Loretnz factor γ and non-linearity parameter $\chi_e \geq 1$.

1.3 STRONG-FIELD QED

Next-generation lasers with multi-PW capability are expected to reach the highly non-linear quantum dominated regime $a_0 \gg 1$ resulting in a so-called QED-plasma [38, 39]. Allowing us to measure extreme non-linear effects in the laboratory, such as a QED-plasma are similar to those found to exist in extreme astronomical environments in the magnetosphere of pulsars [40], crab nebula due to its magnetic field strength [41] and black holes [42]. The electrons in the focus of a strong laser pulse $E_L \sim 10^{13}$ Vm^{-1} with Lorentz factor γ accelerated to ultrarelativistic energies emit gamma-ray photons probabilistically and their motion becomes highly stochastic and unpredictable. Unlike the classical description of radiation reaction in which the electrons emit electromagnetic radiation continuously as described by the self-consistent Landau-Lifshitz (LL) formalism [43].

Understanding the interactions of electrons in strong electromagnetic fields classically is insightful although incomplete as it predicts photons with higher energies than the emitting electrons. Therefore, a fully quantum framework is crucial in order to model the *complete* description of the photon emission and motion of the electrons, as they interact in the regime of strong-field quantum electrodynamics. As a result, the emission process is described using the Furry picture [44] capturing the discrete nature of the emission.

As we have discovered so far, an electron reaching a magnitude comparable to that of E_{crit} is unavailable [45] . It would require a laser intensity called the Schwinger intensity $I_s = 0.5\epsilon_0 c E_s^2 \sim 10^{29}\text{Wcm}^{-2}$, χ_e then becomes $\chi_e \approx \gamma(1+\cos\theta)(I/I_s)^{0.5}$ where θ is a geometrical factor of the propagation angle of the laser to the electron bunch. To overcome the intensity constraint, via a Lorentz boost as the ultra-relativistic electrons counter-propagate, corresponding to $\theta = 0$ to the

laser pulse, electrons can reach $\chi_e \sim 1$ with much lower laser fields $E_L \sim 10^{13}\mathrm{Vm}^{-1}$, where the ratio $E_L/E_{\mathrm{crit}} \sim 10^{-4}$. It is also important to mention that the geometry of the collision plays an important part in reaching high χ_e as an electron accelerated to c along the direction of the pulse, $\mathbf{E}_\perp$ is canceled by the $\mathbf{v} \times \mathbf{B}$ term whereas in an over-dense plasma the term does not cancel. As we will see, in the counter-propagation in the geometry of $\theta = 0$ the two terms add producing an overall factor of two in eqn 1.1 for χ_e . As the value of the electron's χ_e approaches unity, $\chi_e \sim 1$, a substantial fraction of the electron's energy (≈ 0.44) is given to the emitted photons. An estimation for χ_e which shows an energy dependency is

$$\chi_{\mathrm{e}} \sim 0.1 \frac{\mathcal{E}_0}{500\mathrm{MeV}} \sqrt{\frac{I}{10^{21}\mathrm{Wcm}^{-2}}}$$

where $\mathcal{E}_0$ is the initial electron-beam energy illustrates that if the electrons are accelerated externally to energy $\mathcal{E}_0 \geq 500\mathrm{MeV}$ with current petawatt laser intensity $\mathrm{I} \geq 10^{21}\mathrm{Wcm}^{-2}$, the electrons would be accelerated to the non-linear regime of $\chi \geq 0.1$. In fact, much work has been performed [46, 47] in using long pulses to accelerate electrons to GeV energies using laser wakefield acceleration (LWFA) [48]. A wakefield is most suitable to accelerate electrons to ∼GeV energies due to the electrons in a created plasma bubble which are exerted under strong electromagnetic fields.

1.4 OUTLINE

In Chapter 2, the classical description of radiation reaction is provided. I will consider the collision of a Gaussian laser pulse with a counter-propagating electron-beam. I will derive *ab initio* the analytical solution for the evolution of the average electron Lorentz factor as a function of time. This is transformed to the average non-linearity parameter for an electron in a Gaussian temporal envelope. I will also consider other pulse shapes such as pulses with a supergaussian form. I will extend a previous solution for $\langle\gamma\rangle$ but will now depend on the supergaussian order n. I will discuss how the laser pulse duration can influence the magnitude of the non-linearity parameter.

Chapter 3 explores the ideas of quantum effects at $\chi_e \geq 0.1$ that changes the electrons motion as the bunch interacts with the electromagnetic field of the laser pulse $a_0 \gg 1$. I will show using the classical, modified-classical and quantum radiation reaction models that χ_e exhibits identical characteristics to the electron's Lorentz factor. The operations of the particle-in-cell code EPOCH are detailed along with explanation of computing the average χ_e of the electron bunch.

At the end of Chapter 3 we turn to asymmetric Gaussian laser pulses to maximise the electron's non-linearity parameter and electron-positron pair yields. I will show that the fast rising edge of a skewed Gaussian is compensated by the reduction in the peak of the laser intensity. Consequently, I will show how a compressed Gaussian pulse is more conducive to enhancing QED effects over a skewed pulse. The experimental constraints of skewing the temporal envelope of the laser pulse optically or otherwise are considered and results compared with realistic pulses. Lastly, a plasma optics scheme using a plasma mirror to produce a fast rising edge on the leading edge of the pulse is considered.

2

MODELLING CLASSICAL RADIATION REACTION

2.1 COUNTER-PROPAGATING LASER - ELECTRON-BEAM COLLISIONS

Accelerating charges radiate electromagnetic radiation. The law of conservation of energy dictates that a fraction of energy of the electron is taken by an emitted photon. Classically, the electrons radiate continuously along its classical wordline. As a result of a continuous radiation reaction, the momentum $\mathbf{p}$ of the electron changes, where the expectation value of this momentum $\langle \mathbf{p} \rangle$ has been derived previously by N. V. Elkina *et al* [49]. An electron with energy $m_e c^2$ and Lorentz factor γ evolves in time according to the equation

$$m_e c^2 \frac{d\gamma}{dt} = -\mathcal{P}_c \tag{2.1}$$

where $\mathcal{P}_c$ is the classical power

$$\mathcal{P}(\chi_e) = \frac{2\alpha_f c}{3\lambda\!\!\!^{-}_c} m_e c^2 \chi_e^2 g(\chi_e) = \mathcal{P}_c g(\chi_e) \tag{2.2}$$

where $\lambda\!\!\!^{-}_c$ is the reduced Compton wavelength. Observing that the classical power $\mathcal{P}_c$ scales quadratically with χ_e, thus $\mathcal{P}_c \propto \chi_e^2$. Furthermore, the generalised power includes the corrective Gaunt factor $g(\chi_e)$ which will be explained in detail in the modified-classical model 2.2. The χ_e of the electrons scales differently as $g(\chi_e)$ deviates from unity, as classically the scaling is χ_e^2 but eventually becoming $\chi_e^{2/3}$ for $a_0 \gg 1$. The laser pulse is counter-propagating to the electron-beam, therefore with

a Lorentz boost into the electron's rest frame, the components of the electric **E** and magnetic field **B** add thus χ_e gains a factor of two

$$\chi_e = 2\gamma \frac{E_L}{E_{\text{crit}}} \tag{2.3}$$

If we substitute χ_e into the power equation and using the result that in the classical model we assume $g(\chi_e) = 1$ simplifies the equation to

$$\begin{aligned} \mathcal{P}_c(\gamma) &= \frac{2\alpha_f c}{3\lambda\!\!\!^{-}_c} m_e c^2 \left(2\gamma \frac{E_L}{E_{\text{crit}}}\right)^2 \\ &= \frac{8\alpha_f c}{3\lambda\!\!\!^{-}_c} m_e c^2 \gamma^2 \frac{E_L^2}{E_{\text{crit}}^2} \end{aligned} \tag{2.4}$$

Eqn 2.1 can be solved by substituting the classical power and denoting the variable $\tau_R = 3\lambda\!\!\!^{-}_c E_{\text{crit}} / 8\alpha_f c E_L$.

$$\frac{d\gamma}{dt} = -\frac{\gamma^2}{\tau_R}$$

Separating variables and integrating both sides

$$\int \frac{d\gamma}{\gamma^2} = -\int \frac{dt}{\tau_R}$$

$$-\gamma^{-1} + C = -\frac{t}{\tau_R}$$

Letting $\gamma(t=0) = \gamma_0$, the constant $C = 1/\gamma_0$ and solving for γ yields the solution

$$\gamma(t) = \frac{\gamma_0}{1 + \gamma_0 t/\tau_R} \tag{2.5}$$

This is the most simple form of the evolution of the electron's $\gamma(t)$ and is only valid for a constant laser intensity. We have reproduced the result found by M. Vranic *et al* after integrating eqn (8) in [50]. The reduction of the electron's Lorentz factor can be seen in fig 2.1 for a 1GeV electron-beam. At the time $t = 0$, the initial point of the collision, the electrons begin to reduce in energy immediately at this

point, loosing >75% of energy over 100fs. As we observe in this figure, the reduction to the electron's Lorentz factor γ is very rapid and this rate depends on the initial energy of the electrons γ_0 and τ_R which ultimately depends on the electromagnetic field or specifically the ratio E_L/E_{crit}. This solution is only valid for $t > 0$ as $\gamma_0 \to \infty$ for negative values of t. This result will now be extended to a Gaussian laser pulse in which the intensity profile is not constant but is a varying function of time. As we will discover, the solution using a Gaussian envelope is valid for both negative and positive values of t.

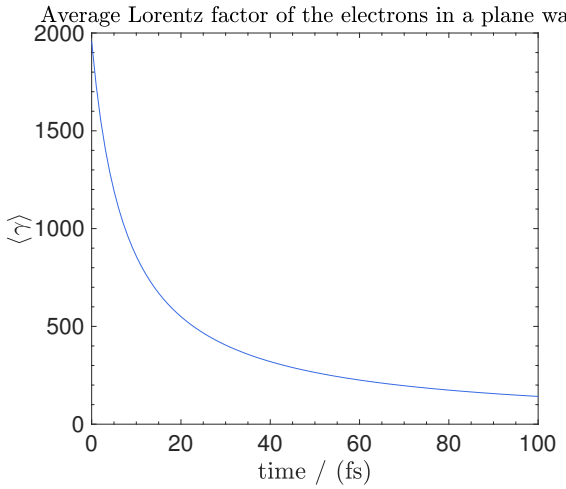

Figure 2.1: Reduction in the electron's Lorentz factor γ in the collision of a 1GeV electron-beam and a constant intensity plane wave using classical radiation reaction.

2.1.1 *Gaussian temporal intensity envelope*

Instead of a constant plane wave, consider the profile of the laser intensity to have a Gaussian form, namely $I(x,t) = I_0 e^{-(x-x_0)^2/L^2}$, which has displacement from the origin at position x_0 at $t = 0$. The laser pulse is counter-propagating in the negative x direction at speed c to the electron-beam so therefore

$$I(x,t) = I_0 e^{-(x+ct-x_0)^2/L^2}$$

The position of the election is x_e, thus $x_e = -x_0 + ct = -(x_0 - ct)$,

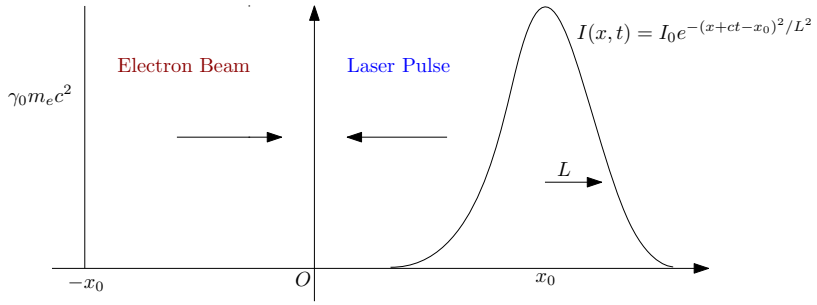

Figure 2.2: A 1D laser pulse that is counter-propagating to an electron-beam. The Laser pulse has a Gaussian intensity envelope and travels at velocity c in the $-x$ direction, while the electron-beam travels in the positive x-direction. The electrons at $-x_0$ are assumed to be monoenergetic, thus with an energy $\mathcal{E}_0 = \gamma_0 m_e c^2$ prior to the collision.

hence the intensity profile at the position of an electron is as follows

$$\begin{aligned} I(x_e, t) &= I_0 e^{-(x_e + ct - x_0)^2/L^2} \\ &= I_0 e^{-(2ct - 2x_0)^2/L^2} \end{aligned}$$

Therefore we find

$$I(x_e, t) = I_0 e^{-4(ct - x_0)^2/L^2}$$

Introducing the term $L' = L/2$ and $ct' = ct - x_0$ then the intensity profile becomes $I(x_e, t) = I_0 e^{(-ct')^2/L'^2} = I_0 e^{t'^2/\tau_L'^2}$. One can define the intensity profile in terms of the laser electric field simply as follows

$$E_L^2 = \frac{I}{\epsilon_0 c} = \frac{I_0}{\epsilon_0 c} e^{-t'^2/\tau_L'^2}$$

$$E_L^2 = E_0^2 e^{-t'^2/\tau_L'^2} \tag{2.6}$$

where the peak electric field E_0 is defined as

$$E_0 = \sqrt{\frac{I_0}{\epsilon_0 c}}$$

which includes I_0, the peak laser intensity, ϵ_0 is the permittivity of free space and c is the speed of light in vacuum. Depending on the polari-

sation of the electric field **E**, a factor of two is necessary for a linearly polarisered wave in the definition of E_0, such that $E_0 = (2I_0/\epsilon_0 c)^{0.5}$. Eqn 2.6 can be substituted into eqn 2.4, where the power radiated by the electron becomes

$$\mathcal{P}_c(\gamma) = \frac{8\alpha_f c}{3\lambda\!\!\!^{-}_c} m_e c^2 \gamma^2 \frac{E_0^2}{E_{\text{crit}}^2} e^{-t'^2/\tau_L'^2}$$

Defining the instantaneous power as a function of the Lorentz factor γ

$$\mathcal{P}_c(\gamma) = -\frac{\gamma^2 m_e c^2}{\tau_R} e^{-t'^2/\tau_L'^2} \tag{2.7}$$

where τ_R denotes the constant with typical order $\tau_R \sim 10^{-11}$ for a peak electric field of $E_0 \approx 1.37 \times 10^{14}\text{Vm}^{-1}$

$$\tau_R = \frac{3\lambda\!\!\!^{-}}{8\alpha_f c} \left(\frac{E_{\text{crit}}}{E_0}\right)^2 \tag{2.8}$$

Substituting eqn 2.7 into 2.1 gives the first-order differential equation

$$\frac{d\gamma}{dt} = -\frac{\gamma^2}{\tau_R} e^{-t'^2/\tau_L'^2}$$

Separating variables and integrating

$$-\int_{\gamma_0}^{\gamma} \frac{d\gamma}{\gamma^2} = \frac{1}{\tau_R} \int_{-\infty}^{t'} dt e^{-t'^2/\tau_L'^2}$$

Letting $t'' = t'/\tau_L'$ gives $dt'' = dt'/\tau_L'$ and integrating the left-hand-side

$$\frac{1}{\gamma} - \frac{1}{\gamma_0} = \frac{\tau_L'}{\tau_R} \int_{-\infty}^{t'/\tau_L'} dt'' e^{-t'''^2} \tag{2.9}$$

This integral takes the form of the error function $\text{erf}(x)$, which has the formal integral definition

$$\text{erf}(x) = \frac{2}{\sqrt{\pi}} \int_0^x e^{-t^2} dt \tag{2.10}$$

We can split the integral up as follows and use eqn 2.10

$$\begin{aligned}\int_{-\infty}^{t'/\tau'_L} dt'' e^{-t''^2} &= \int_{-\infty}^{0} dt'' e^{-t''^2} + \int_{0}^{t'/\tau'_L} dt'' e^{-t''^2} \\ &= \frac{\sqrt{\pi}}{2} + \frac{\sqrt{\pi}}{2}\text{erf}\left(\frac{t'}{\tau'_L}\right)\end{aligned}$$

Using this result along with the left-hand-side of eqn 2.9, we may solve for the Lorentz factor γ giving

$$\frac{1}{\gamma} - \frac{1}{\gamma_0} = \frac{\tau'_L}{\tau_R}\frac{\sqrt{\pi}}{2}\left[1 + \text{erf}\left(\frac{t'}{\tau'_L}\right)\right]$$

$$\frac{\gamma_0}{\gamma} = 1 + \frac{\sqrt{\pi}\tau'_L\gamma_0}{2\tau_R}\left[1 + \text{erf}\left(\frac{t'}{\tau'_L}\right)\right]$$

Therefore we find that our solution for the average Lorentz factor of the electron bunch is

$$\frac{\gamma}{\gamma_0} = \frac{1}{1 + \frac{\sqrt{\pi}\tau'_L\gamma_0}{2\tau_R}\left[1 + \text{erf}\left(\frac{t'}{\tau'_L}\right)\right]}$$

$$\langle\gamma(t)\rangle = \frac{\gamma_0}{1 + \delta\left[1 + \text{erf}\left(\frac{t}{\tau_L}\right)\right]} \tag{2.11}$$

where δ is a parameter dependent on the peak electric field E_0, half of the pulse duration $\tau_L = 0.5\tau_p$ and initial γ factor given by

$$\delta = \frac{\sqrt{\pi}\tau_L\gamma_0}{2\tau_R}$$

Now we may discover how the electron's energy evolves after entering the Gaussian laser pulse. Eqn 2.11 is shown in fig 2.3 where the effects of classical radiation reaction becomes noticeable. In this figure, the electrons enter the laser pulse at time $t = -60$fs and loose an average of 75% of energy to continuous photon emission and resulting classical radiation reaction. At the time $t = 0$, the electrons are at the peak of the envelope, with no longer enough energy to emit and therefore radiation reaction is no longer altering the electrons dynamics. It can

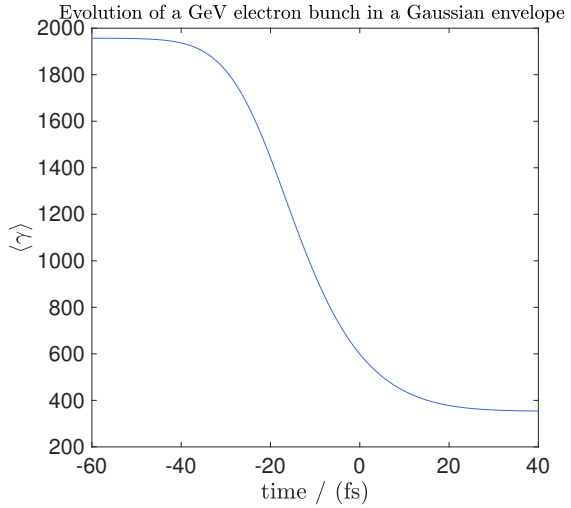

Figure 2.3: Evolution of a 1GeV, where $\gamma = 1957$ electron bunch entering a Gaussian laser pulse. The average Lorentz factor γ of the electron's derived in eqn 2.11 for pulse durations $\tau_p = 40$fs. Noting this solution approximates eqn 2.5 for large values of τ_p.

be seen in this figure that this occurs at 20fs at which point the electrons average Lorentz factor is $\langle\gamma\rangle \approx 400$ or 208MeV. The continuous loss of energy of the electrons to each emitted photon, as described in section 1.2.3 can be as much as $0.44\chi_e\gamma mc^2$ [51]. Although, we will shortly discover that this classical description is an over estimate of the emission by electrons and a scaling factor is introduced leading to the modified-classical model. In this figure, we gain insight into the symmetry of the laser pulse as the electrons enter the pulse with γ_0 and leave the pulse having lost significant energy due to classical radiation reaction. Taking the derivative of eqn 2.11 we find

$$\frac{\mathrm{d}}{\mathrm{dt}}\langle\gamma\rangle = -\frac{\gamma_0^2\exp(-t^2/\tau_L^2)}{\tau_R(1+\delta(1+\mathrm{erf}(t/\tau_L^2)))^2} = -\frac{(\gamma(t))^2}{\tau_R}\times\frac{E_L^2}{E_0^2} \tag{2.12}$$

We find that this expression is simply the instantaneous power radiated $-\mathcal{P}/m_ec^2$, arriving back at the original eqn 2.1 showing the validity of eqn 2.11 as a Gaussian pulse is employed.

We have plotted the derivative of the electron's Lorentz factor in fig. 2.4 which highlights two effects. Namely, that higher energy elec-

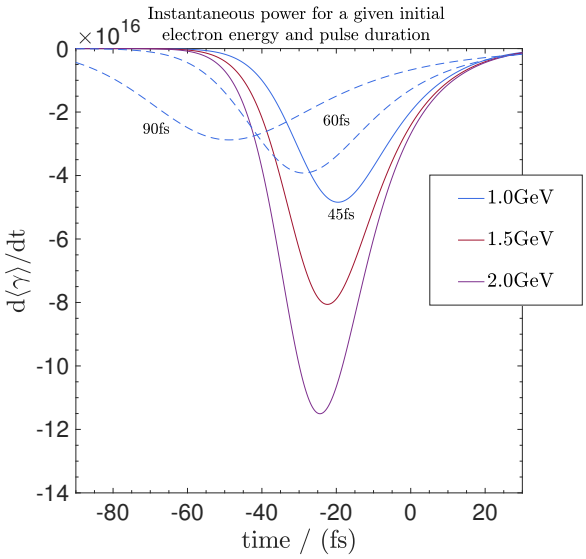

Figure 2.4: Equation 2.12 showing the derivative of the Lorentz factor of the electrons for different electron energies $\mathcal{E}_0$ and three laser pulse durations τ_p.

trons in the pulse will emit higher energy photons and therefore lose energy more rapidly using the classical radiation reaction model. Secondly, compressing the laser pulse to shorter pulse durations our model predicts that the electron's $\langle\gamma\rangle$ reduction becomes more significant.

The average non-linearity parameter $\langle\chi_e\rangle$ may be derived simply from the relation $\chi_e = \gamma E_L / E_{\text{crit}}$ and from multiplying $\langle\gamma\rangle$ in eqn 2.11 by the factor $2E_0 \exp(-t^2/2\tau_L^2)/(E_{\text{crit}})$ to find the average χ_e of the electron bunch for a Gaussian pulse

$$\langle\chi_e\rangle = \frac{\chi_0 \exp(-t^2/2\tau_L^2)}{1 + \delta(1 + \text{erf}(t/\tau_L))} \tag{2.13}$$

where χ_0 is the electron's initial non-linearity parameter before entering the pulse (at $t = -\infty$). This result is plotted in fig 2.5 along with the energy of the electron bunch for a short 40fs laser pulse with intensity $2 \times 10^{21}\text{Wcm}^{-2}$ colliding with a GeV electron beam. This result for χ_e also agrees with that found in equation (7) in [52], although in terms of phase of the pulse $\chi_e(\phi)$. Similarly, we can take the derivative of the average χ_e.

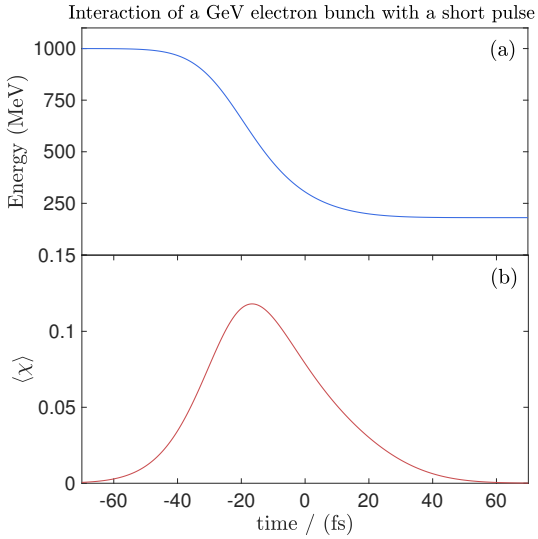

Figure 2.5: Evolution of a GeV electron bunch showing (a) the energy in MeV and (b) average non-linearity parameter χ_e of the electrons for an ultra-short 40fs pulse.

The derivative is important because it provides the time in which the average χ_e of the electrons is maximised in the laser pulse

$$\frac{\mathrm{d}}{\mathrm{dt}}\langle\chi_e\rangle = \frac{\chi_0}{\xi^2}\left(\frac{\xi t}{\tau_L^2}\exp(-t^2/2\tau_L^2) + \frac{\gamma_0}{\tau_R}\exp(-3t^2/2\tau_L^2)\right) \tag{2.14}$$

where we are denoting $\xi = 1 + \delta(1 + \mathrm{erf}(t/\tau_L))$. The derivative has been plotted in fig 2.6 for three initial electron energies $\mathcal{E}_0$ from 1GeV-2GeV. We can deduce from this result that the initial energy of the electron beam (initial γ_0) plays a crucial role in maximum $\langle\chi_e\rangle$ and also shifts the time in which χ_e is maximised, $\mathrm{d}\langle\chi_e\rangle/\mathrm{dt} = 0$. This is due to the electrons loosing energy to radiation reaction at different rates. This can be seen in the definition of χ_e in eqn 2.3, as χ_e is proportional to *both* the magnitude of the laser electric field and the electron's initial Lorentz factor, γ_0.

Our analytical model shows that the maximum peak $\langle\chi_e\rangle$ for a GeV electron beam is $\langle\chi_e\rangle \approx 0.12$ and increases to in excess of $\langle\chi_e\rangle \approx 0.18$ for a 2GeV beam. Those electrons which have a high γ and are at the peak of the pulse would therefore be influenced by quantum effects as the

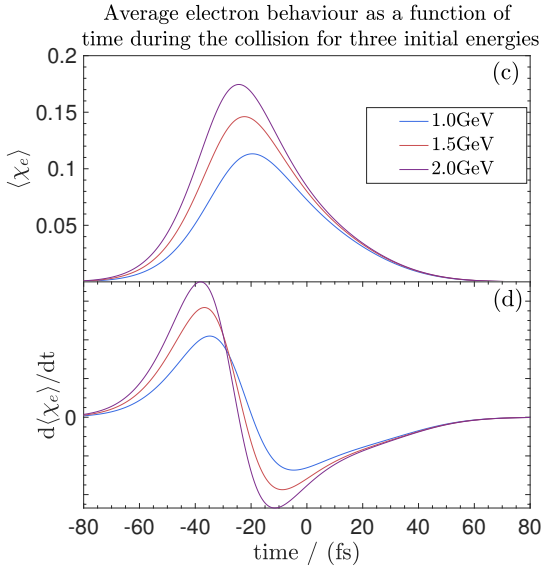

Figure 2.6: Evolution of the non-linearity parameter. (c) peak average χ_e for an electron bunch with three initial energies. $\mathcal{E}_0$ (d) eqn 2.14 showing the derivative of $\langle\chi_e\rangle$ parameter. We observe χ_e is maximised for higher initial energy of the electron beam, the derivative shows the time in which χ_e is maximum which is before the peak.

electrons have a $\chi_e \geq 0.1$. To describe what we have found, consider an impossible situation in which the radiation reaction effect was turned off, the peak would indeed be the point at which χ_e is a maximum as this is the point of maximum field strength. However, as the electrons are losing energy in the pulse to radiation, the center is therefore not the point of maximum χ_e.

We have considered laser and electron-beam parameters that are realised with current laser systems and future facilities. As mentioned previously, the classical description of radiation reaction overestimates the photon emission at high values of χ_e. Therefore, these results show only the approximate evolution of the electrons and may be improved on by using a modified-classical model.

Now that we have derived a solution for the average electron's χ_e, consider a solution in which the envelope is skewed. If the peak intensity of the pulse I_0 is constant, we would expect the curves in fig. 2.6 to shift as the time in which the electrons reach the peak would be shorter. If the peak intensity I_0 was reduced to I_1 after skewing the laser envelope,

the electrons would therefore have a higher $\langle\gamma\rangle$ but would observe a lower laser field. The influence on χ_e therefore will be determined by the competition between the average γ and the laser intensity.

2.1.2 *Extending our solution to a supergaussian laser pulse*

Suppose we now extend our solution given by eqn 2.13 to a generalised supergaussian laser pulse. The laser electric field takes the general form $E_L(t) = E_0 \exp(-((t-t_0)/\tau_p)^n)$, where n is the order of the supergaussian at an arbitrary initial time t_0. The supergaussian pulse shape has the characteristic in which the peak is less smooth and boxed for larger values of the positive integer constant n as shown in fig. 2.7. Following the derivation of section 2.1.1, however now with the generalised n-th order laser electric field, we arrive at the general solution for the average Lorentz factor of the electrons

$$\langle\gamma_n(t)\rangle = \gamma_0\left(1 + \frac{2\tau_L\gamma_0}{\tau_R}\left[\Gamma\left(\frac{n+1}{n}\right) - \frac{t}{2n\tau_L} E_{((n-1)/n)}\left(\frac{t}{\tau_L}\right)^n\right]\right)^{-1} \tag{2.15}$$

where $\Gamma(n)$ denotes the gamma function and $E_n(t/\tau_L)$ is the exponential integral with a non-integer order. This solution is plotted for the Gaussian pulse $n = 2$ in fig. 2.8 showing that this equation predicts the result of equation 2.11. However, eqn 2.15 produces undesired results for odd n and suggests the electron's leave the pulse having lost all energy to radiation reaction, $\gamma = 0$ for $t > 0$ shown in fig 2.8. This may be because this solution does *not* take the modulus inside $E((t-t_0)/\tau_L)$ as $(t-t_0)^3$ where $t < t_0$, would cause the exponential integral to diverge.

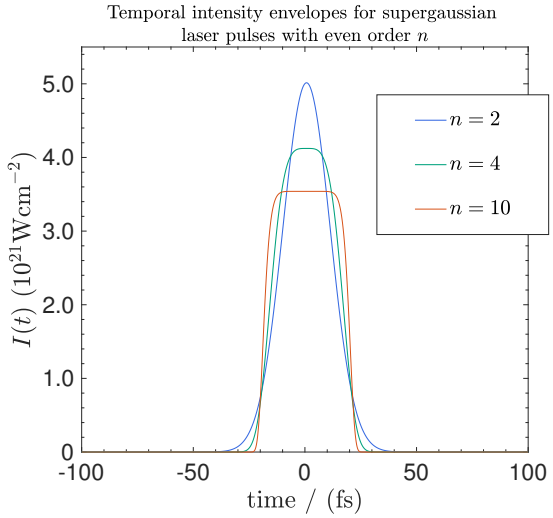

Figure 2.7: Laser intensity profile $I(t)$ of a supergaussian shape for integer values of the order n. For $n > 2$, a Gaussian, the profile becomes a top hat function for increasing values of the order parameter n.

Using the particle-in-cell code, we may choose any value of n. However, we will only focus on even values for n. We can use the PIC code to determine the maximum non-linearity parameter the electrons reach inside the supergaussian envelope.

$$\text{PIC } \langle \chi_e \rangle = \langle \gamma_n(t) \rangle \frac{E_L(n,t)}{E_{\text{crit}}}$$

The maximum value of the electron's $\langle \chi_e \rangle$ for different values of the order parameter n is provided in table 2.1. The number of electron-positron pairs produced per electron $N_\pm / N_e$ after the collision with the laser has also been measured. Enhancement in the pair density has been considered using a supergaussian $n = 5$ characteristic envelope [53]. N. Abdukerim finds that as the supergaussian order changes from 1-5, pair numbers change from 7.21×10^{-3} to 9.36×10^{-3}. Although a small increase, it is mentioned that a shorter pulse length can encourage higher pair yields. This will be tested in section 2.1.4, where we will see the effect that the pulse duration has on the non-linearity parameter.

As we have discovered so far in this chapter, the time in which the electrons reach the peak is important in maximising χ_e. Since χ_e de-

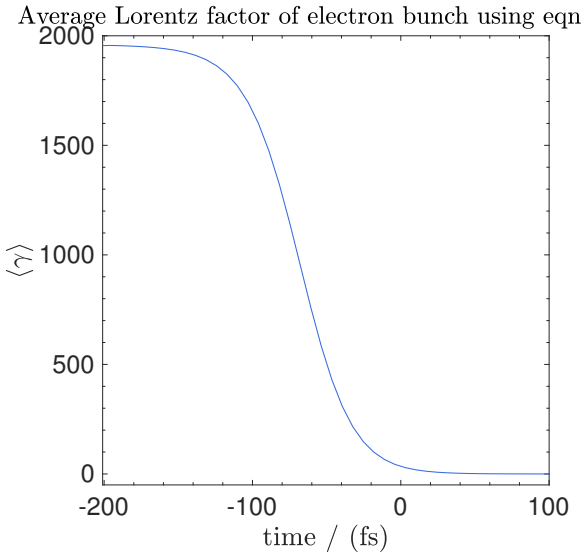

Figure 2.8: Lorentz factor of the electrons predicted by eqn 2.15 using a Gaussian $n = 2$ laser pulse with intensity $2 \times 10^{21}\text{Wcm}^{-2}$ and pulse duration 60fs colliding with a 1GeV electron-beam.

n	$\mathcal{R}_s$	$\langle\chi_e\rangle$	$N_\pm/N_e(10^{-5})$
2	1	0.402	2.1609
4	0.822179	0.4660	1.9554
6	0.758202	0.4952	2.9788
8	0.725649	0.5054	2.8920
10	0.705980	0.5073	2.8850
12	0.6928	0.5063	2.8418

Table 2.1: Simulating a $5 \times 10^{21}\text{Wcm}^{-2}$ supergaussian laser pulse with parameter n measuring the e^-e^+ pairs produced per electron as the order n is increased. The amplitude I_0 of the intensity envelope is reduced to conserve the total energy in the pulse.

pends of γ, the supergaussian intensity profile may reduce the loss of energy to radiation reaction due to the increase in the rising edge of the pulse. We have used the PIC code to calculate the number of electron-positron pairs produced after the collision of a 1.5GeV electron-beam with a 40fs, $5 \times 10^{21}\text{Wcm}^{-2}$ supergaussian envelope. The parameter n was varied from a Gaussian to essentially a flat-top intensity envelope a maximum for $n = 12$.

The results of these simulations are provided in table 2.1 showing maximum average χ_e and pair yields. Discovering that maximum aver-

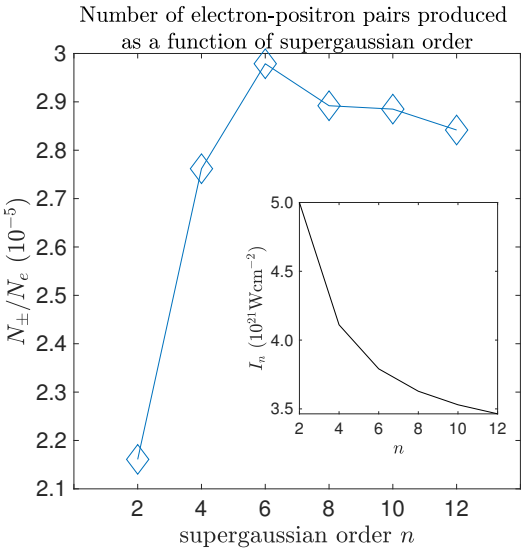

Figure 2.9: Number of electron-positron pair yields per electron as a function of the supergaussian order parameter n. The inset gives an indication of how the peak I_n is reduced as n is increased and the envelope becomes further modified as the pulse energy is conserved.

age χ is increased by ≈ 0.1 as the envelope becomes increasing steeper. Fig. 2.9 shows how the pair yields are influenced as a function of the supergaussian order. We find a small but increasing pair yield per electron for increasing values of n. This increase however, does not continue above a maximum of $n = 6$ with pair yields of 2.9788×10^{-5} and slowly tails off as the envelope becomes a 'top-hat' function $n = 12$, giving electron-positron pair yields per electron of 2.8418×10^{-5}. The number of pairs produced per electron in these simulations are small overall therefore indicating that the leading edge of the supergaussian envelope does not play a significant role in pair enhancement. In section 3.4 we will see if these results hold by applying a significantly faster rising edge at the front leading edge of the laser pulse.

2.1.3 *Normalising the electric field*

If we wish to conserve the total energy of the pulse, i.e the integral of $I(t)$ or $E(t)^2$ over all times, we need to consider the normalisation constant. Let I_n be the peak amplitude of the intensity of the laser field with a supergaussian temporal envelope of the general form $I(t) = I_n \exp(-(t/\tau_p)^n)$, the total energy in the pulse is therefore

$$\mathcal{E} \propto \int_{-\infty}^{\infty} I(t)\ dt = \int_{-\infty}^{\infty} E^2(t)\ dt$$

Following the full derivation given in appendix A.1, we find that the peak intensity I_n varies with the order n according to

$$I_n = \frac{2^{1/n} n\sqrt{\pi}}{2^{3/2}\Gamma(1/n)} I_0 = \mathcal{R}_s I_0$$

In order to test this relation, letting $n = 2$ gives

$$I_2 = \frac{2^{1/2} 2\sqrt{\pi}}{2^{3/2}\Gamma(1/2)} I_0 = \frac{2^{1/2}\sqrt{\pi}}{2^{1/2}\sqrt{\pi}} I_0 = I_0$$

Therefore, the energy in the supergaussian is conserved by the temporal envelope defined by

$$I(t) = \mathcal{R}_s I_0 \exp(-(t/\tau_p)^n) \tag{2.16}$$

Figure 2.7 shows the intensity spectrum $I(t)$ for a Gaussian, $n = 2$, $n = 4$ and $n = 10$ supergaussian envelopes. It is important to note that the energy in the three envelopes are conserved. This is the formalism that is used in our PIC code simulations in order to produce the results of the previous section.

2.1.4 *A look at parameters to influence the non-linearity parameter*

Laser parameters play a crucial role in producing electrons with high magnitudes of χ_e. We observe this by considering the dependency χ_e has on the laser full-width at half-maximum (FWHM). This is achieved by comparing maximum peak average χ_e of the electron bunch with our analytical result 2.13 to simulation results. We will explain the particle-in-cell code EPOCH used in these simulations in section 3.3. We find that reducing the FWHM by compressing the laser pulse duration produces electrons with higher magnitudes of χ_e. Simulating a variety of short and longer pulse durations, fig 2.10 shows the change in peak average χ_e. The laser pulses with a longer pulse duration of 150fs are similar to the long pulses that will be used on the L4 ELI beam line [54].

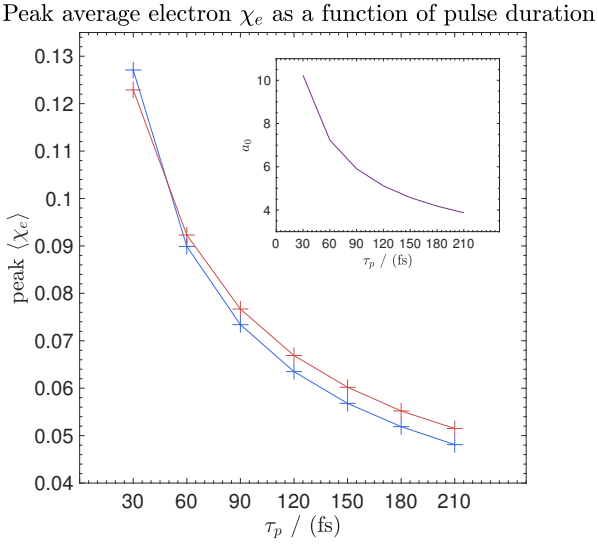

Figure 2.10: Peak average χ_e of a 1.5GeV electron bunch with $\gamma_0 = 2931$ as a function of laser pulse duration τ_p using the classical radiation reaction model, eqn 2.13 (blue) and simulation (red). (inset) The corresponding reduction in the normalised vector potential parameter a_0 as a change in laser pulse duration τ_p.

We have seen previously that the non-linearity parameter depends on the intensity profile and the position of the electron's in the pulse.

Therefore, χ_e is maximised for electron's at regions of the highest intensity. Increasing the FWHM of the laser pulse and therefore the intensity profile is reduced, the magnitude of χ_e decreases. It is thus important to use a short pulse duration and compress the laser pulse to reach high magnitudes of χ_e. Let us now justify why this is indeed true.

Firstly, consider a generalised Gaussian beam described by the intensity profile

$$I(r) = r_0 \exp\left(-2\frac{r^2}{w^2}\right)$$

where r_0 is the peak amplitude and $2w$ is the full width and related to the FWHM by

$$2w = \frac{\sqrt{2}\text{FWHM}}{\sqrt{\ln 2}}$$

This relation shows the linear proportionality $w \propto$ FWHM between our laser pulse duration and the width of a generalised profile $I(r)$. Therefore, the width of $I(r)$ is proportional to w^2, in the limit as $w \to \infty$ the pulse becomes shorter.

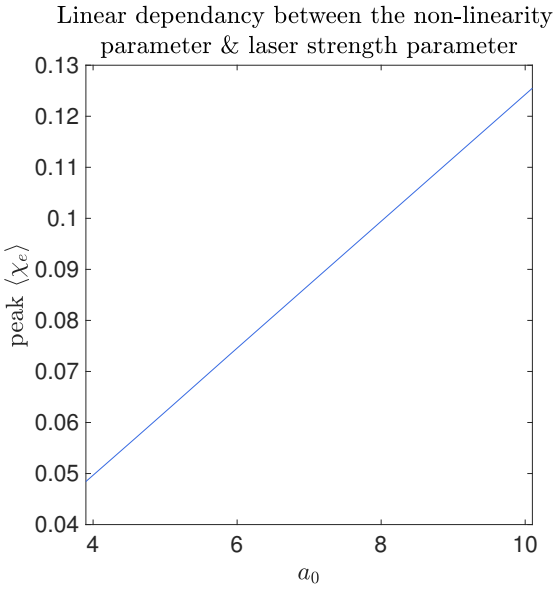

Figure 2.11: Peak average χ_e of a 1.5GeV electron bunch with a $\gamma_0 = 2931$ as a function of laser strength parameter a_0.

We can also observe this in the inset of fig 2.10 which shows how the value of a_0 changes as a function of laser pulse duration τ_p from

our PIC code simulation. This shows clearly the laser strength parameter reduction if we increase our laser pulse duration. The relationship between a_0 and laser intensity is $a_0 \propto I^{0.5}$ given by

$$a_0 = \frac{eE}{m_e c\omega} = 0.85\sqrt{\frac{I}{10^{18}\mathrm{Wcm}^{-2}}}\left(\frac{\lambda}{\mu\mathrm{m}}\right)$$

where e is the electron charge, ω is the laser frequency, E is the electric field, m_e is the mass of the electron and c is the speed of light in vacuum. A drop in the laser intensity because of an increase in τ_p will also result in a smaller a_0. As we have seen previously, χ_e scales linearly with the strength of the laser field a_0, so fig 2.10 is an intuitive illustration of how χ_e varies with τ_p, the laser pulse duration. We see in this plot that both our analytical model and PIC agree reasonably within errors between the two models. Illustrated in fig 2.11 is the corresponding linear scaling of χ_e with a_0 from the results provided in fig 2.10. Finding a factor of 2 increase in average χ_e from a strength parameter of $a_0 = 4$ to $a_0 = 10$, highlighting the importance of high a_0 through reducing the pulse duration. This result found follows that observed by Harvey *et al* [55] with electron straggling, whereby the electron's χ_e is not reduced in the focus of shorter laser pulses attributed to electrons reaching the centre of the pulse without radiating away energy.

Another important consideration is the geometry of the collision to maximise χ_e. For an electromagnetic wave at an angle θ to the electron-beam $\chi_e = \gamma(t)E_L(1+\cos\theta)/E_{\mathrm{crit}}$. T. G. Blackburn *et al* [56] suggests that contrary to intuition where χ_e is maximum for $\theta = 0$ in the factor $1+\cos\theta$, in fact in certain conditions the optimum angle to observe certain QED effects is at normal incidence to the electron-beam.

2.2 MODIFIED-CLASSICAL EMISSION EQUATIONS

The modified-classical equations of motion for large Lorentz factor γ, conserves the energy of the electrons which the classical model fails to do. As the electrons in the intense external laser field are influenced by stochastic emission, i.e emission that can no longer be well predicted by deterministic equations such as 2.11 and 2.13, corrections to the synchrotron spectrum are therefore crucial to avoid overestimating the emission process. Accounting for corrections to the emission spectrum in particle-in-cell codes have also been widely adopted. The crystals experiment at CERN measured the transition between classical and quantum synchrotron theory finding electrons with energies $> 100\text{GeV}$ ($\gamma \sim 10^5$). The experiment, at the CERN SPS H4 beamline used a Germanium crystal because they provide strong electric fields $\sim 10^{11}\text{Vcm}^{-1}$, where quantum synchrotron emission can be measured. As a result of this experiment the Gaunt factor [57] for synchrotron radiation was measured [58] and is given by

$$g(\chi_e) = \frac{\int_0^{\chi/2} F(\chi_e, \chi_\gamma) d\chi_\gamma}{\int_0^{\infty} F_c\left(\frac{4\chi_\gamma}{3\chi_e^2}\right) d\chi_\gamma} = \frac{3\sqrt{3}}{2\pi\chi_e^2} \int_0^{\chi_e/2} F(\chi_e, \chi_\gamma) d\chi_\gamma \tag{2.17}$$

where the function $F(\chi_e, \chi_\gamma)$ is the quantum synchrotron function $F(\chi_e, \chi_\gamma)$ provided by A. A. Sokolov and I. M Ternoc [59]

$$F(\chi_e, \chi_\gamma) = \frac{4\chi_\gamma^2}{\chi_e^2} y K_{0.66}(y) + \left(1 - \frac{2\chi_\gamma}{\chi_e}\right) y \int_y^{\infty} K_{1.66}(t) dt \tag{2.18}$$

where $y = 4\chi_\gamma / (3\chi_e(\chi_e - 2\chi_\gamma))$ and K_n are modified Bessel functions of the second kind. In the classical limit as $g(\chi_e)$ and $h(\chi_e)$ are exactly unity, $F(\chi_e, \chi_\gamma)$ reduces to the classical synchrotron function $F_c(\chi_e, \chi_\gamma)$

$$F_c(\chi_e, \chi_\gamma) = y_c \int_{y_c}^{\infty} K_{1.66}(u) du$$

where the term y_c is $4\chi_\gamma/3\chi_e^2$ including χ_γ and χ_e which are the usual non-linearity parameters for the photon and electron respectively.

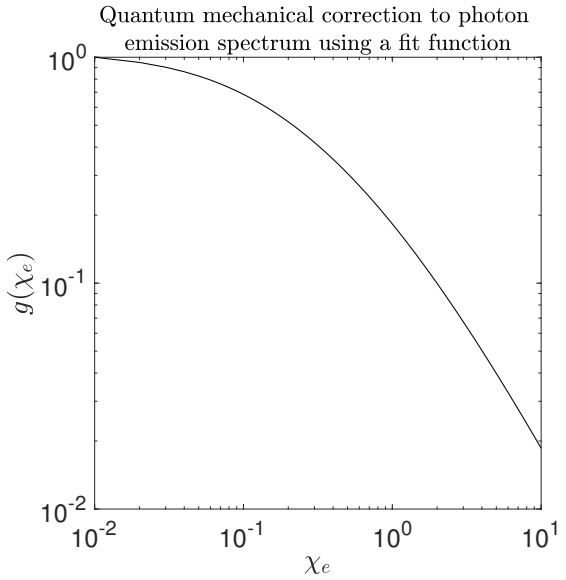

Figure 2.12: Estimate of quantum mechanical correction to the synchrotron power given by eqn 2.19 on a logarithmic scale.

For $\chi_e \ll 1$, $g(\chi_e)$ is approximated by the polynomial [60]

$$g(\chi_e) \approx 1 - \frac{55\sqrt{3}}{16}\chi_e + 4.8\chi_e^2$$

and for values $\chi_e \gg 1$, $g(\chi_e) \approx 0.5564\chi_e^{-4/3}$ [36]. An estimation over the whole range of χ_e values is the following V. N. Baier *et al* [61]

$$g(\chi_e) = [1 + 4.8(1+\chi_e)\ln(1+1.7\chi_e) + 2.44\chi_e^2]^{-2/3} \tag{2.19}$$

This fit function $g(\chi_e)$ is plotted in fig 2.12 over the full range of χ_e values $10^{-2} \leq \chi_e \leq 10^1$. Note that the two expressions of $g(\chi_e)$ in the limits for $\chi \ll 1$ and $\chi \gg 1$ arise from eqn 2.19, however for $\chi \ll 1$ the coefficient on the χ_e term is only an approximation not derived from 2.19. The incorporation of $g(\chi_e)$ in the equation of motion eqn 2.1 for classical radiation reaction corrects the instantaneous power function as $\mathcal{P} \propto \chi_e^2$ is unbounded. As the non-linearity parameter χ_e approaches unity, $g(\chi_e) = 0.2$, therefore the instantaneous radiated

power is reduced by a factor of 5. The correction of $g(\chi_e)$ to the photon emission spectrum assuming a constant crossed field, where the weak-field approximation is valid may be applied to our model.

$\mathcal{E}_0$	$I(10^{21})\mathrm{Wcm}^{-2}$	τ_p (fs)	Peak $\langle\chi_e\rangle$	Facility
1	3	30	0.2677	Gemini
50	0.1	100	2.5322	SLAC
4	100	10	3.2386	ELI
4	20	15	2.2649	APOLLON

Table 2.2: Comparing the peak average χ_e for laser parameters found at current and next-generation multi-PW laser facilities.

In order to model the quantum corrected $\langle\chi_e\rangle$ in eqn 2.13, we would need to integrate the power of the electrons in eqn 2.2 but with the inclusion of $g(\chi_e)$ from eqn 2.19. Although this has not been derived analytically, we may use our PIC code to see the difference between χ_e classically ($g(\chi_e) = 1$) and χ_e with quantum corrections ($g(\chi) < 1$), shown in fig. 3.6. It can be seen that the peak $\langle\chi_e\rangle$ is increased by $\chi_e \sim 0.05$ using the modified-classical and quantum models compared to the classical solution.

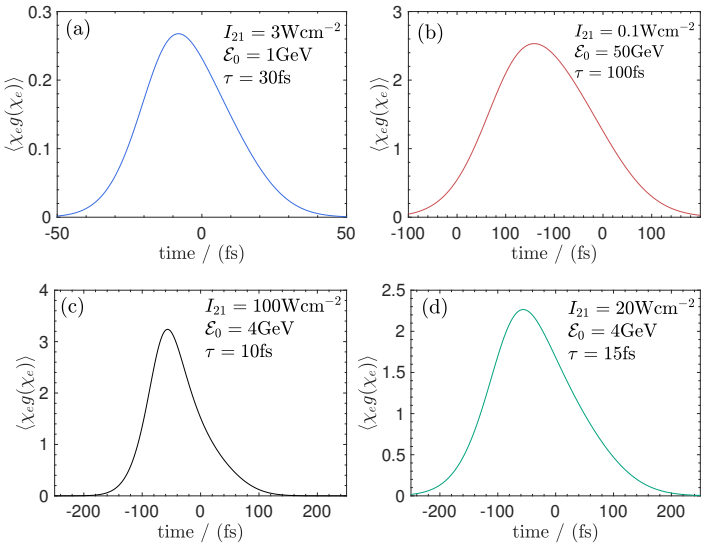

Figure 2.13: Comparing quantum corrected $\langle\chi_e\rangle$ with current experimental parameters (a) Gemini and (b) SLAC and next-generation ELI (c) and (d) APOLLON, Laboratoire d'Utilisation des Lasers Intenses (LULI). Results are provided in table 2.2

We can now use the quantum corrected average χ_e to predict the behaviour in the evolution of the electrons at current and upcoming laser facilities. These results can be seen in table 2.2 and are plotted in fig 2.13. The SLAC parameters are taken from the SLAC 50 GeV linac, the Final Focus Test Beam (FFTB). We are assuming that the laser is linearly polarised, with wavelength of 1μm and FWHM given by τ_p. The interplay between initial electron energy $\mathcal{E}_0$ and laser intensity is seen in these results, highlighting that both are equally crucial in miximising $\langle\chi_e\rangle$. The values of $\langle\chi_e\rangle$ presented here are in agreement with the simulation results in T. G. Blackburn *et al* [52].

3

QED EFFECTS FOR $a_0 \gg 1$

3.1 MODELLING QUANTUM RADIATION REACTION

Deciding which radiation reaction model is most suitable to describing the electrons after the collision with the laser pulse is crucial. As we have discovered the classical radiation reaction model is a deterministic process, becoming probabilistic at $a_0 \gg 1$. Equations 2.11 and 2.13 derived earlier are therefore only approximations and assumes that the photon emission is continuous. The modified-classical model corrects the emitted photon spectrum by scaling the amount of energy a photon may take from an electron, while conserving the electron energy. The quantum radiation reaction model we will consider includes the discontinuous nature of the photon emission. This is achieved using the quasi-static weak-field approximations along with the Monte-Carlo algorithm described in section 3.3. The choice of using the quantum radiation reaction model in this research is primarily due to the spread in the electron χ_e distributions in the collision with the pulse. This means that the photon emission is no longer continuous and As we will shortly discover, the evolution of the electrons drastically change as the quantum radiation reaction model is considered.

3.1.1 *Quasi-static weak-field approximations*

In order to model QED processes for $a_0 \gg 1$, we adopt the quasi-static weak-field approximations described by V. I. Ritus [62]. We use the

quasi-static approximation for synchrotron-like emission in both the classical and modified-classical models. Firstly, the weak-field approximation assumes that our electromagnetic laser field is less than the critical field $E_L < E_{\text{crit}}$, which is a valid assumption since $E_L \leq 10^{-3} E_{\text{crit}}$ is limited by current generation laser systems. We also assume the probabilistic emission rates depend only on χ_e and not the field invariants $\mathcal{F}$ and $\mathcal{G}$, where

$$\begin{aligned} \chi_e &= \frac{e\hbar}{m_e^2 c^4} |F_{\mu\nu} p^\nu| \quad & \chi_\gamma &= \frac{e\hbar^2}{2m_e^3 c^3} |F^{\mu\nu} k_\nu| \\ \mathcal{F} &= -\frac{F_{\mu\nu} F^{\mu\nu}}{2E_{\text{crit}}^2} & \mathcal{G} &= -\frac{F^*_{\mu\nu} F^{\mu\nu}}{4E_{\text{crit}}^2} \end{aligned} \tag{3.1}$$

provided that both $\mathcal{F}, \mathcal{G} \ll 1$ and also that $\chi_e^2 \gg \text{Max}(\mathcal{F}, \mathcal{G})$ [63]. The corresponding vector forms of the four invariants are given by

$$\begin{aligned} \chi_e &= \frac{\gamma |\mathbf{E}_\perp + \mathbf{v} \times \mathbf{B}|}{E_{\text{crit}}} \quad & \chi_\gamma &= \frac{\hbar |\omega \mathbf{E}_\perp + c^2 \mathbf{k} \times \mathbf{B}|}{2 m_e c^2 E_{\text{crit}}} \\ \mathcal{F} &= \frac{\mathbf{E}^2 - c^2 \mathbf{B}^2}{E_{\text{crit}}^2} & \mathcal{G} &= \frac{\mathbf{E} \cdot c\mathbf{B}}{E_{\text{crit}}^2} \end{aligned} \tag{3.2}$$

where $\mathbf{v}$ is the velocity of the electron with Lorentz factor γ, E_{crit} is the critical field $E_{\text{crit}} = m_e^2 c^3 / q_e \hbar$, $\mathbf{E}$ and $\mathbf{B}$ are the external electric and magnetic fields with $\mathbf{E}_\perp$ the electric field perpendicular to $\mathbf{v}$. The invariant χ_γ is analogous to χ_e, however the non-linearity parameter for a photon with wave vector $\mathbf{k}$, frequency ω and energy $\hbar\omega$. If the electron is in its rest frame $\mathbf{v} = 0$, $\gamma = 1$ and $\chi_e = 1$ then the electron will observe the critical field E_{crit}. The quasi-static approximation is used to ensure that the formation length of the emitted hard photons are smaller than the external background field, such that the fields in which the emission occurs are considered as constant.

3.1.2 *Moment equations*

The emission operators for classical and quantum radiation reaction are defined by C. P. Ridgers *et al* [64]. For classical emission continuously which is analogous to (2.1)

$$\frac{\partial f}{\partial t} = \frac{1}{p^2}\frac{\partial}{\partial p}\left(p^2 \frac{P_{cl}}{c} f\right) \tag{3.3}$$

where f is the electron distribution function, p is the momentum of the electron and P_{cl} is the classical instantaneous power. For a stochastic radiation reaction, this result becomes

$$\frac{\partial f}{\partial t} = -\lambda_\gamma(\chi_e) f + \frac{b}{2m_e c}\int_p^\infty dp' \lambda_\gamma(\chi_e')\rho_{\chi_\gamma}(\chi_e', \chi_\gamma)\frac{p'^2}{p^2} f(\mathbf{p}') \tag{3.4}$$

Assuming $\chi_e = \gamma b$, where $b = |\mathbf{E}_\perp + \mathbf{v} \times \mathbf{B}|/E_{\text{crit}}$ given f is the distribution of the electrons, λ_γ is the rate of photon emission with probability that an electron emits a photon $\rho_{\chi_\gamma} d\chi_\gamma$ with parameter χ_γ.

The first and second moments of (3.3) for classical radiation reaction and (3.4) for quantum radiation reaction describe how the electron's energy distribution evolves in time. These are found by multiplying either equation by γ or γ^2 respectively and integrating. Building on work previously undertaken using an electron-beam with Gaussian distribution colliding with a plane electromagnetic wave in [64], it is shown that from the first moment the electron's $\langle\gamma\rangle$ decreases most rapidly for classical RR and evolves identically for the modified-classical and quantum RR models. The second moment shows that the width of the energy distribution narrows for both classical and modified classical, with the former model narrowing most rapidly. This is intuitive because higher energy electrons can emit photons with higher energies. However, the quantum model shows that the width of the electron energy distribution can decrease but also increase in time, a characteristic

that is impossible with the other radiation reaction models. This is a direct consequence of the stochastic nature of quantum radiation reaction at $a_0 \gg 1$ with electrons that have a $\chi_e \geq 0.1$. We may reproduce these results now with the non-linearity parameter $\langle \chi_e \rangle$.

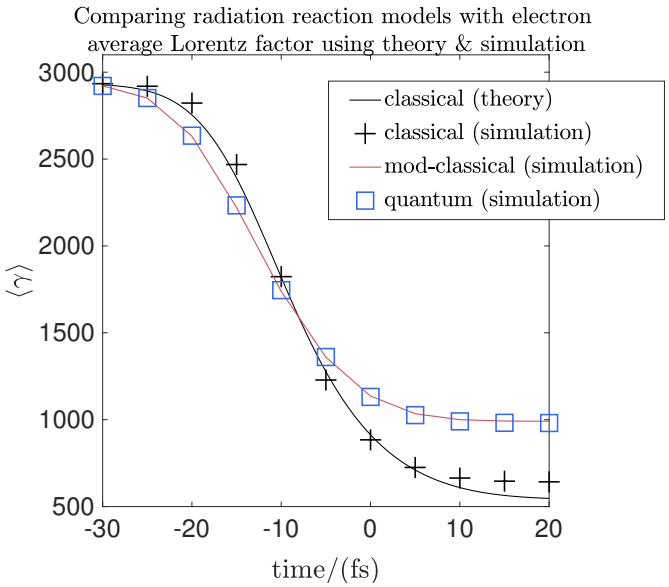

Figure 3.1: Average Lorentz factor as a function of time using the three radiation reaction models. Results are identical to those in [64], however by changing the pulse from a plane electromagnetic wave to a Gaussian pulse profile.

Indeed, fig. 3.1 reproduces the behaviour found in [64] identically for the electron's Lorentz factor $\langle \gamma \rangle$ but with a Gaussian laser electric field profile. Furthermore, fig. 3.2 shows the standard deviation on the electron's χ_e distribution for classical, modified-classical and quantum radiation reaction models. As expected, σ in the quantum case increases, reaching maximum $\chi_e \approx 0.13$ and then decreases, whereas for classical and modified-classical, the electron's σ tends to zero. This is because of the stochasticity observed in the quantum RR model that is not possible for classical or modified-classical RR.

These results have been plotted using both the prediction from our model in eqn 2.11 and also compared with PIC code simulation which are both in agreement for classical RR. The PIC code uses the Monte-

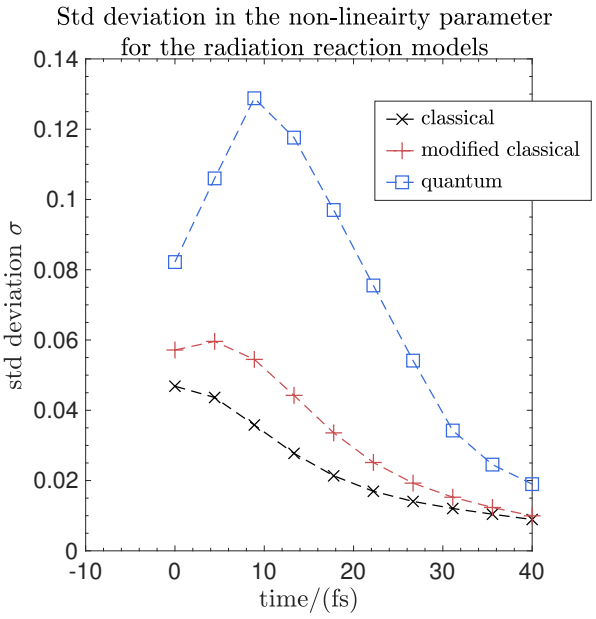

Figure 3.2: Standard deviation σ in the non-linearity parameter χ_e for classical, modified-classical and quantum RR models, agreeing with previous results found for the electron's Lorentz factor γ in [64].

Carlo algorithm to model the emission and is described in section 3.3. They are important because they detail the regimes of radiation reaction and that maximising the electron's χ_e will truly depend on how stochastic the electrons become as they approach $\chi_e \sim 1$. Modelling this stochasticity is detailed in the competition between the two terms produced from the moment equations in [64]

$$T_+ = \frac{\langle S \rangle}{m_e^2 c^4} \quad T_- = 2\frac{\langle \Delta\gamma g(\chi_e) P_c \rangle}{m_e c^2}$$

where, S is an integral over χ_e^4, P_c is the classical radiated power and $\Delta\gamma = \gamma - \langle\gamma\rangle$. The ratio of these two terms $\xi = T_+/T_-$ at the beginning of the collision enables us to determine the stochasticity of the electrons and therefore the characteristic signatures of quantum radiation reaction. The first experimental signatures of radiation reaction in an all-optical experiment has recently been performed using the Gemini laser system conducted by J. M. Cole *et al* [9]. In simulations performed in their set-up, signatures of quantum effects would

be visible at $\chi_e \approx 0.25$. Measuring the electron and photon spectra, experimental data indicates signatures of quantum RR. It is clear from these results that current laser systems are on the edge of measuring quantum radiation reaction.

3.2 BREIT-WHEELER PAIR PRODUCTION

The Breit-Wheeler process is the production of an electron-positron pair from the collision of two photons, $\gamma\gamma' \rightarrow e^- e^+$ [65]. This process can be seen in fig. 3.3, in which a photon with wavevector k and non-linearity parameter χ_γ decays into an electron-positron pair with momentum p and non-linearity parameter χ_- and χ_+ respectively.

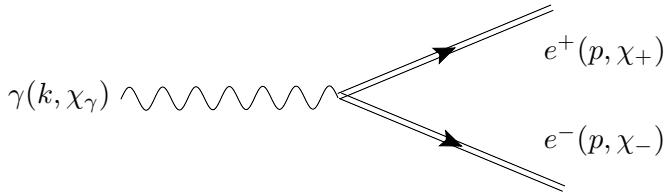

Figure 3.3: Diagram of Breit-Wheeler electron-positron pair production. A photon with wave vector k and efficiency parameter χ_γ interacts with the background laser field to produce an electron-positron pair with momentum p and non-linearity parameter χ_- and χ_+ respectively.

Consider the differential probability rate that a photon with χ_γ decays into an electron-positron pair with efficiency parameters $\chi_\pm$

$$\frac{\mathrm{d}W_\pm}{\mathrm{d}\chi_+} = \frac{\alpha_f}{\tau_c}\frac{m_e c^2}{\hbar\omega}\chi_\gamma \frac{\mathrm{d}T(\chi_\gamma)}{\mathrm{d}\chi_+}$$

where α_f is the fine structure constant, τ_c is the Compton time and $h\omega$ is the photon energy for photons with χ_γ. Integrating over the positron efficiency parameter χ_+ gives our probability rate

$$W_\pm = \frac{\alpha}{\tau_c}\frac{m_e c^2}{\hbar\omega}\chi_\gamma T(\chi_\gamma) \tag{3.5}$$

where the function $T(\chi_\gamma)$ has been defined by Erber *et al* [36]

$$T(\chi_\gamma) = \begin{cases} \frac{3\sqrt{3}}{8\sqrt{2}} \exp\left(-\frac{4}{3\chi_\gamma}\right) & \chi_\gamma \ll 1 \\ 0.60\chi_\gamma^{-1/3} & \chi_\gamma \gg 1 \end{cases} \tag{3.6}$$

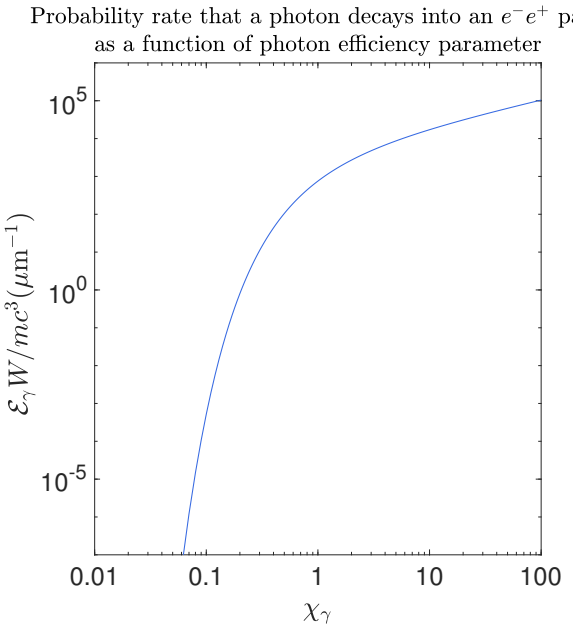

Figure 3.4: Predicting the probability rate $W_\pm$ that a photon with energy $\mathcal{E}_\gamma$ decays into an e^-e^+ pair from (3.5) and using $T(\chi_\gamma)$ from (3.6) for values of the photon efficiency parameter over the range $0 \leq \chi_\gamma \leq 100$.

The pair probability rate is plotted in fig 3.4 for a given photon efficiency parameter. We find that the pair rate drastically increases as χ_γ approaches unity, $\chi_\gamma \sim 1$ with copious pairs $\sim 10^5$ at $\chi_\gamma \gg 10$.

3.3 SIMULATING LASER - ELECTRON-BEAM COLLISIONS

This research employs the particle-in-cell (PIC) code EPOCH [66] to simulate the interaction of the colliding laser - electron-beam. EPOCH 1D is used for simplicity but can be extended to 2D or 3D simulations by including extra dimensions to the simulation domain and laser pulse. However, constraining the simulations to only 1D removes any instabilities that can arise in higher dimensions. PIC codes are ubiquitous to simulate plasma physics and comprise of essentially two solvers. The first solver calculates the electromagnetic fields and currents due to the charged particles as they move in space. This process is numerically solving Maxwell's equations on a spacial grid using a finite-difference time-domain (FDTD) scheme on a Yee staggered grid. The FDTD scheme uses a leapfrog scheme in which the fields $\mathbf{E}$ and $\mathbf{B}$ are updated at half $n + 1/2$ time-steps, namely

$$\mathbf{E}^{n+1/2} = \mathbf{E}^{n} + \frac{\Delta t}{2}\left(c^2 \nabla \times \mathbf{B}^{n} - \frac{\mathbf{J}^{n}}{\epsilon_0}\right) \tag{3.7}$$

$$\mathbf{B}^{n+1/2} = \mathbf{B}^{n} - \frac{\Delta t}{2}\left(\nabla \times \mathbf{E}^{n+1/2}\right) \tag{3.8}$$

and then at full time-steps $n + 1$

$$\mathbf{E}^{n+1} = \mathbf{E}^{n+1/2} + \frac{\Delta t}{2}\left(c^2 \nabla \times \mathbf{B}^{n+1} - \frac{\mathbf{J}^{n+1}}{\epsilon_0}\right) \tag{3.9}$$

$$\mathbf{B}^{n+1} = \mathbf{B}^{n+1/2} - \frac{\Delta t}{2}\left(\nabla \times \mathbf{E}^{n+1/2}\right) \tag{3.10}$$

Meanwhile the current $\mathbf{J}^{n}$ is updated between the half and full time steps Δt. The particle pusher solves the particles relativistic equation of motion under the relativistic Lorentz force law. The PIC code operations are illustrated in fig 3.5 below. In the following simulations the laser is circularly polarised with wavelength of $\lambda = 1\mu$m and enters the domain from the left-hand-side boundary. The polarisation is achieved

by using two lasers in which the phase of one of the lasers is displaced by $\pi/2$. The electron-beam is monoenergetic and propagates from the right-hand-side boundary of the simulation box.

The radiation reaction module takes the positions and momenta of the particles as well as the local values of the electromagnetic fields and calculates the radiation reaction on the electrons (and positrons) using various models described previously: classical in chapter 2, modified-classical in section 2.2 or full QED in chapter 3. The placement of this module within the PIC loop shown in fig 3.5 determines the accuracy of the solution. For simplicity the module is currently placed at the start of the time loop. This is found to be adequate in convergence testing of our results, as discussed later. This is still an active area of research as inclusion and accuracy of classical radiation reaction models a PIC code has been compared by M. Vranic *et al* [67]. The simulation model that this research is concerned with however is primarily the QED-PIC in order to simulate pair production and quantum radiation reaction. QED effects in the PIC code are simplified by assuming the weak field approximation, 3.1.1. Namely, the low frequency fields are treated as constant during emission and the fields are weaker than the critical field E_{crit}. The probabilistic nature of the emission process is coupled to the PIC code and works self-consistently as the QED-PIC, employing the Monte-Carlo algorithm.

The extended PIC code that uses the Monte-Carlo algorithm is described in depth by C. P. Ridgers *et al* [68] and has been used to study QED effects in [69]. Similar numerical QED simulations have been performed without the use of a Monte-Carlo algorithm [70] to simulate multiple pair production. The Monte-Carlo algorithm uses the theory of Poisson statistics by assigning an optical depth τ to each particle emitted with probability $P = 1 - \exp(-\tau)$. The pseudoparticle is given a final optical depth in the probability range $P = [0, 1]$ and is

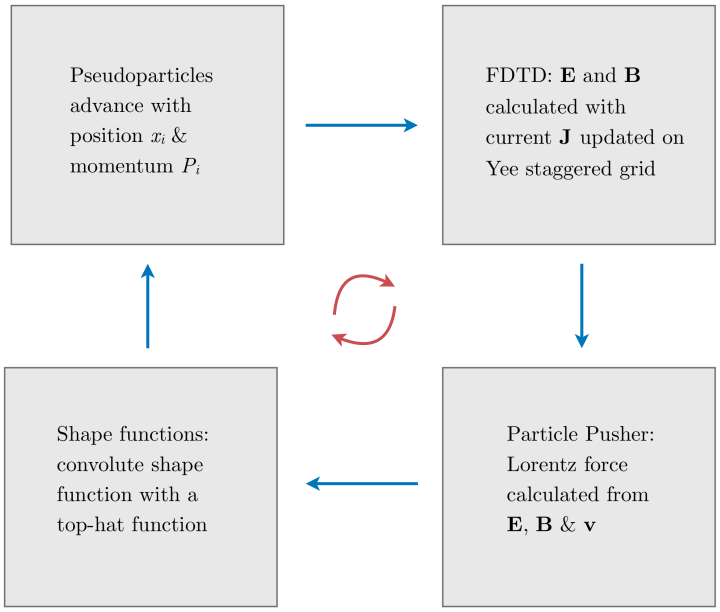

Figure 3.5: Core operations involved in a particle-in-cell (PIC) code as described in T. D. Arber *et al* [66]. The finite difference time domain (FDTD) is the technique used to solving Maxwell's equations numerically as the fields are advanced.

integrated along the electron's trajectory until the final optical depth is reached. The electron emits a photon at the final optical depth when the condition $\tau \equiv \tau_{\text{final}}$ is satisfied.

We now consider the simple algorithm used to calculate the value of the electron's χ_e. The magnitude of χ_e is calculated from eqn 2.3. The components of the electric field are calculated from evaluating $|\mathbf{E}| = (E_x + E_y + E_z)^{1/2}$. This is the local magnitude of the electric field produced by the laser and experienced by the electron for each grid cell. The following operations are performed:

- From the total laser field $|\mathbf{E}|$, each component of laser electric field, E_x, E_y and E_z is calculated.
- We assume the electron bunch is monoenergetic therefore all the electrons enter the pulse with γ_0, χ_0 and momentum p_0 where,

$$\gamma_0 = \sqrt{1 + \left(\frac{p_0}{m_e c}\right)^2}, \qquad \chi_0 = \gamma_0 \frac{E_0}{E_{\text{crit}}}$$

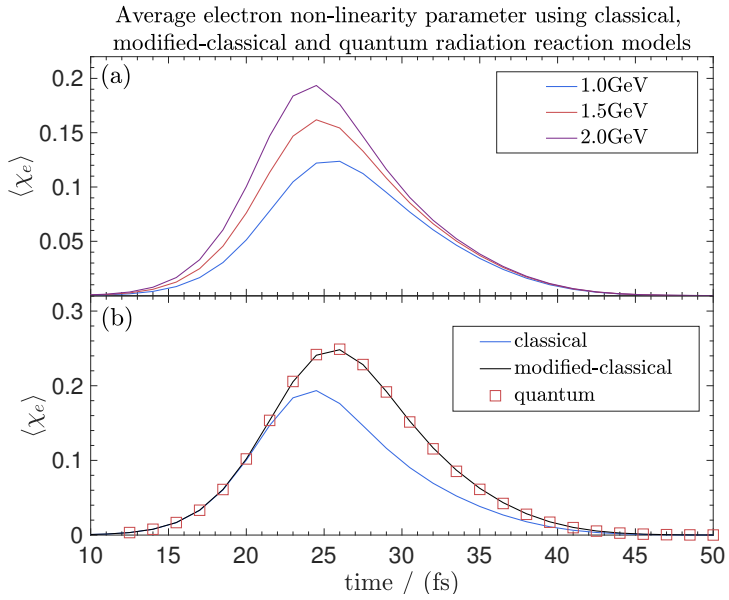

Figure 3.6: Average χ_e of an electron bunch using energies 1.0, 1.5 and 2.0GeV using a 60fs Gaussian laser pulse (a). Comparing $\langle\chi_e\rangle$ using the radiation reaction models, classical, modified-classical and quantum described in section 3.1.2 (b).

- The calculation is simplified since the electrons can be found in the same cell and therefore an average of the electron's χ_e can be calculated from the position of the electrons in each grid cell.

- If however, the electrons enter the pulse with different γ_0, χ_0, the electron bunch will be displaced on the simulation grid. The average of the electron's χ_e will vary depending on which radiation reaction model is considered.

Employing this method to calculate the average χ_e of the electron bunch, we are able to verify the validity of our model in eqn 2.13 with the PIC code. Both the analytical solution along with our simulation evolution of the electron's $\langle\chi_e\rangle$ are compared in fig. 3.7. Both models agree with each other, therefore showing that our analytical model is a valid prediction of the evolution of the electron's average χ_e in a Gaussian pulse.

Plotted in fig 3.6 shows how the radiation reaction models, classical, modified-classical and quantum can be used to determine how $\langle\chi_e\rangle$

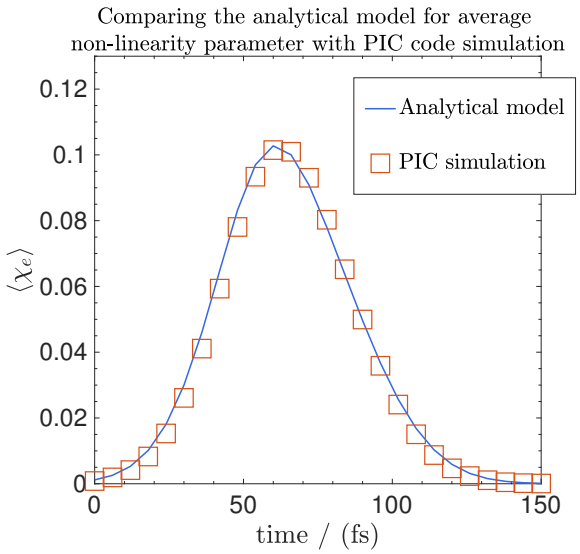

Figure 3.7: Comparing eqn 2.13 with particle-in-cell code simulations using the classical radiation reaction model for a 40fs laser pulse colliding with 1GeV electrons.

evolves. This figure also confirms the identical average behavior in $\langle \chi_e \rangle$ for the modified-classical and quantum RR models as expected from 3.1 shown in section 3.1.2.

3.3.1 *QED-PIC method*

In turn, we will consider two methodologies for simulating the collision of the electron-beam with an asymmetric Gaussian laser pulse with both a fast rising edge at the front of the pulse and a slowly rising edge at the back of the pulse corresponding to a negative and positive skew respectively.

Method 1: exploits the symmetric shape of the Gaussian laser pulse. Essentially, this method changes the temporal pulse duration on either side of t_0 in order to create a positively or negatively rising laser pulse. Applying this difference in the pulse duration τ_p allows one to produce a sharp leading rise at the front (or a slow rising front and a sharp trailing end) of the laser pulse. Consider the laser intensity profile as a piecewise defined Gaussian function

$$I(t) = \begin{cases} I_1 \exp(-(t-t_0)^2/\tau_r^2) & \tau_r > t_0 \\ I_1 \exp(-(t-t_0)^2/\tau_f^2) & \tau_f < t_0 \end{cases} \tag{3.11}$$

where I_1 is related to the peak electric field by

$$I_1 \propto c\epsilon_0 E_1^2 \tag{3.12}$$

Assuming that the laser pulse propagates counter to the electron-beam from the left-hand boundary. If $\tau_r < \tau_f$, we find that the pulse has a sharp fast rising leading edge. Once both are equal, namely by setting $\tau_r \equiv \tau_f$ in eqn 3.11, the laser envelope resolves to a symmetric Gaussian. Figure 3.8 shows this method employed for a Gaussian envelope with energy $\mathcal{E}_1$ and a negatively skewed envelope with energy $\mathcal{E}_2$. The values of the rise and fall time were $\tau_r = 10$fs and $\tau_f = 160$fs giving a reduction to the peak intensity by 53%.

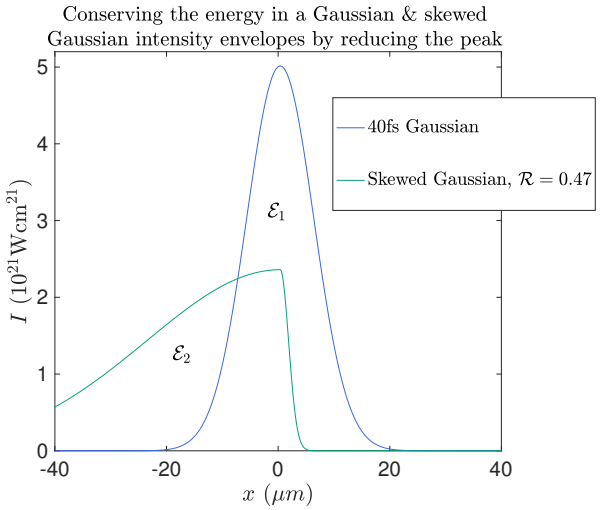

Figure 3.8: Applying *method one* to the particle-in-cell code. Temporal intensity envelopes for a compressed $5 \times 10^{21}\mathrm{Wcm}^{-2}$ 40fs Gaussian laser pulse with energy $\mathcal{E}_1$ along with a negatively skewed envelope with energy $\mathcal{E}_2$.

The energy in both the asymmetric and Gaussian laser envelopes need to remain constant. We therefore assume that optically skewing the pulse will always result in a reduction to the peak intensity in order to conserve energy in the pulses. This approach is used in our PIC code simulations, namely, we scale the intensity profile of the skewed envelope accordingly by a dimensionless ratio $\mathcal{R}$, which is derived as follows. The energy in the pulse is given by

$$\mathcal{E} \propto \int_{-\infty}^{\infty} I_0 \exp\left(-(t/\tau_p)^2\right)\, dt = I_0 \tau_p \sqrt{\pi}$$

From the general relation

$$\int_{-\infty}^{\infty} \exp\left(-x^2\right)\, dx = \sqrt{\pi}$$

Consider now splitting the integral into two separate integrals in terms of τ_r and τ_f, the energy now becomes

$$\begin{aligned}\mathcal{E} &= \int_{-\infty}^{0} I_1 \exp(-(t/\tau_r)^2) + \int_{0}^{\infty} I_1 \exp(-(t/\tau_f)^2) \\ &= \frac{1}{2}\left(\int_{-\infty}^{\infty} I_1 \exp(-(t/\tau_r)^2) + \int_{-\infty}^{\infty} I_1 \exp(-(t/\tau_f)^2)\right) \\ &= \frac{1}{2}\sqrt{\pi}(\tau_r + \tau_f)\end{aligned}$$

Setting the two energies equal for a Gaussian and skewed Gaussian gives

$$I_0 \tau_p \sqrt{\pi} = \frac{1}{2} I_1 \sqrt{\pi}(\tau_r + \tau_f)$$

Rearranging to find the ratio of intensities gives

$$\mathcal{R} = \frac{I_1}{I_0} = \frac{2\tau_p}{(\tau_r + \tau_f)}$$

Giving a new reduced peak, $I_1 = \mathcal{R} I_0$. Including the reduction factor $\mathcal{R}$ is necessary as it ensures that the total energy in a skewed laser pulse for arbitrary values of τ_r and τ_f is conserved, i.e satisfying the relation

$$\int_{-\infty}^{\infty} I(t)dt - \int_{-\infty}^{\infty} I_1(t)dt = 0 \tag{3.13}$$

If the reduction $\mathcal{R}$ was omitted and the temporal envelope remained identical for the skewed envelope, the energy of the laser photons would be unequal to the Gaussian laser photons, thus changing pair yields. We also impose the following condition in the choice of values for the rise time τ_r and fall time τ_f such that

$$2\tau_p < \tau_r + \tau_f \tag{3.14}$$

in order to ensure that $\mathcal{R} < 1$ to give $I_1 < I_0$ avoiding large values $\mathcal{R} \gg 1$. Figure 3.8 shows that after scaling by $\mathcal{R}$ as the rising edge becomes further skewed, the energies remain equal, thus $\mathcal{E}_1 \equiv \mathcal{E}_2$ and

both conditions in 3.14 and 3.13 are satisfied. In order to accurately model this reduction, experimental data would need to be measured and compared with the PIC code. We may understand how rapidly the factor $\mathcal{R}$ reduces the peak of the pulse for given values of the parameters τ_r and τ_f in figure 3.9. This modelling of the peak shows that, in the extreme case of a maximum skew, the peak intensity I_0 is reduced by more than half of the initial compressed envelope, namely $1 - \mathcal{R} = 56\%$.

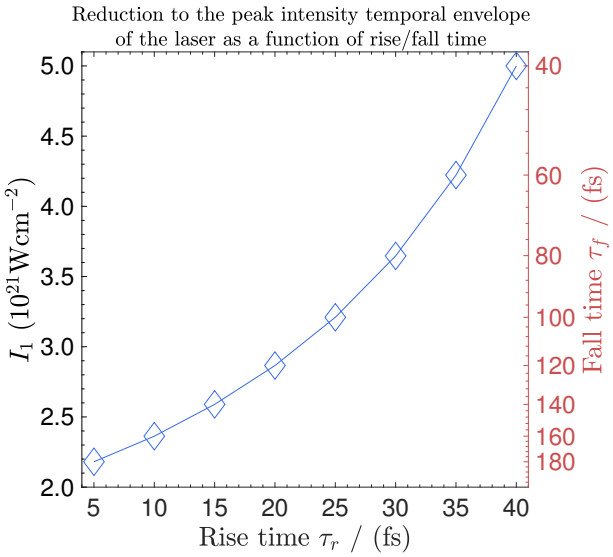

Figure 3.9: Conserving the energy in the modified pulse. The peak temporal intensity envelope is reduced for given values for the rise time τ_r and fall time τ_f respectively.

The QED-PIC simulations that have been performed use the simulation parameters: a domain which is $-100\mu\text{m} \leq x \leq 100\mu\text{m}$ with 10^3 global number of grid points. The laser which has a wavelength of 1μm (50 cells per wavelength) with intensity $5 \times 10^{21}\text{Wcm}^{-2}$ and is circularly polarised. The pulse duration used in the simulations is the e-folding time which is defined by $\tau_L = 0.5\tau_p$, half the total pulse duration. The number of pseudo particles used is 10^3 (20 particles per cell) and the total simulation time is 600fs with a timestep of 2.5fs using simple laser boundary conditions. The electron-beam is monoenergetic with initial beam energy of 1.5GeV and initial density $n_{e0} = 1.8 \times 10^{18}\text{m}^{-3}$.

Method 2: arbitrarily modifies the intensity profile of the laser by a different *skew* parameter, β. The skewed Gaussian is well fitted to the experimental temporal intensity profile in [71] given by

$$I(\beta, t) = I_0 \exp\{-t^2/(2\tau_p^2)[1 + \beta t/(t^2 + \tau_p^2)^{0.5}]^{-1}\} \tag{3.15}$$

where I_0 is the peak intensity and the range of the skew parameter $\beta \in [-1, 1]$. For a Gaussian pulse $\beta = 0$ i.e no skew. A value of $\beta = -1$ produces a fast rise at the leading front edge of the pulse and slow trailing edge at the back of the pulse. $\beta = 1$ corresponds to the inverse profile in which the leading edge has a slow rise and the trailing edge has a fast rise. The advantage of this method is that we have an analytical form for the asymmetric intensity temporal envelope of the pulse, although this method omits the reduction in the peak intensity. The respective shapes of the laser pulse can be seen in fig 3.10 using eqn 3.15 but for the normalised laser electric field E_L.

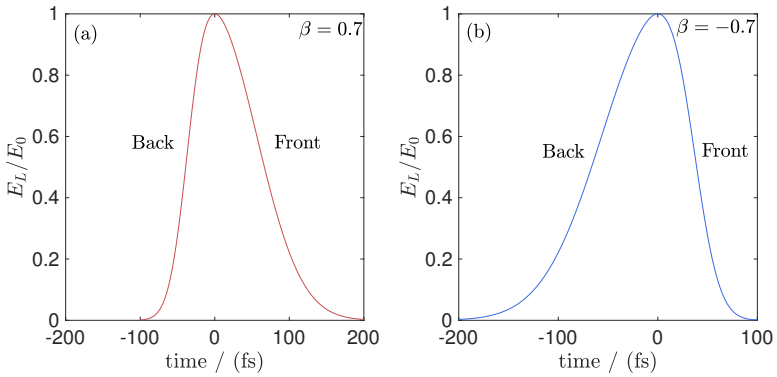

Figure 3.10: Skewing the laser pulse using eqn 3.15 but with the electric field of the laser E_L with positive skew $\beta = 0.7$ in (a) and negative skew in (b) where $\beta = -0.7$. N.B the electron-beam propagates from the right-hand boundary counter to the laser pulse.

The electric field lines are also plotted in fig 3.11, where we observe the higher gradient field lines of the laser field. Observing this figure, we see that the electrons entering the pulse from the right-hand boundary of $\beta = -1$ would reach the highest field gradient and then lower

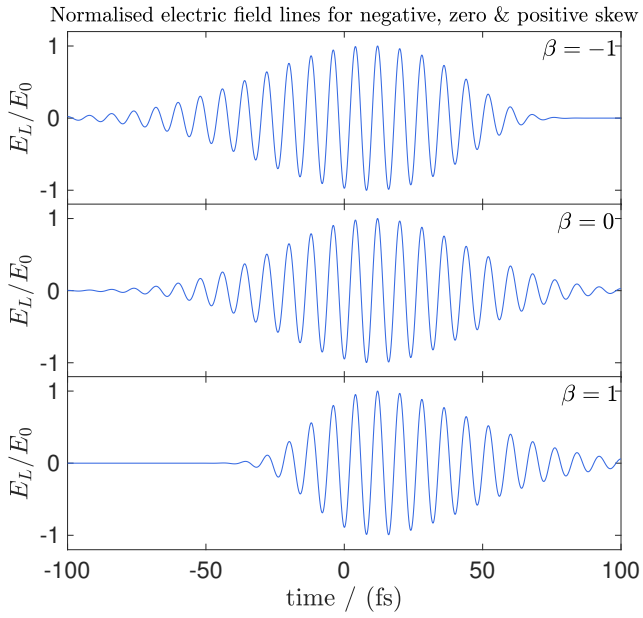

Figure 3.11: Normalised temporal envelope of the electric field $E_L(t)$ of a 45fs Gaussian, $\beta = 0$, positive skewed, $\beta = 1$ and negative skewed, $\beta = -1$ laser pulse used in the particle-in-cell code simulations.

electric field lines after reaching the peak of the pulse. This explains the behavior of the electron's $\langle \chi_e \rangle$ in fig 2.6 for $\beta = 0$ as the electrons reach the peak of the pulse and decrease smoothly reducing in energy.

3.4 THE EFFECT OF PULSE SKEWING

3.4.1 *Maximising the electron non-linearity parameter*

Values of the electron's χ_e are dependent on the strength of the laser field given by the definition of χ_e in the weak field approximation in section 3.1.1. This is justified since χ_e scales linearly with the normalised vector potential a_0 and the electric field by $a_0 \propto E$, using $I(t) = \epsilon_0 c E(t)^2$ one deduces that $\chi_e \propto C\sqrt{I}$, where C is a constant.

This result is plotted in fig 3.12 as predicted by our classical equation using 2.0GeV electrons and a 40fs laser pulse with given intensities in 2.13, agreeing with the result found in fig 2. of [69] for a continuous radiation reaction. Furthermore, χ_e becomes linearly proportional to the laser intensity if the electrons are subject to a discontinuous emission under quantum RR due to hardening of the photon spectrum.

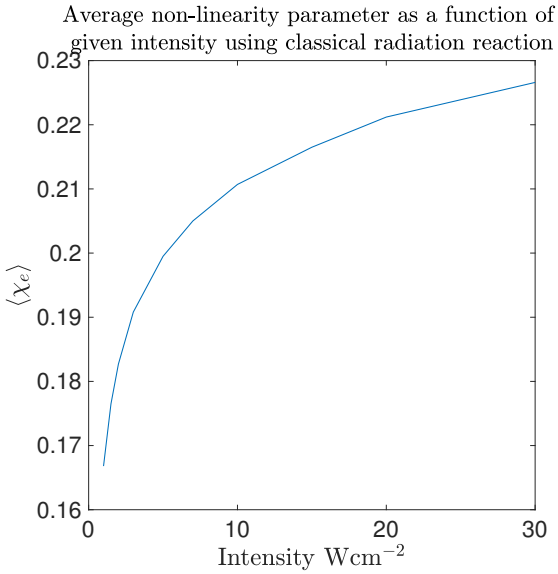

Figure 3.12: Average χ_e as a function of given laser intensity using eqn 2.13, χ_e scales as the square root of the intensity with classical radiation reaction, peak $\langle\chi_e\rangle \propto \sqrt{I(t)}$, becoming $\langle\chi_e\rangle \propto I(t)$ for quantum radiation reaction ($\chi_e \geq 0.1$).

We have seen that the gradient of the laser pule profile becomes important in maximising the non-linearity parameter χ_e. So far, in sec-

tion 2.1.4 it has been shown that the laser pulse duration can also influence magnitudes of the non-linearity parameter. Now we will determine whether the electron's χ_e can be increased if an asymmetric Gaussian intensity envelope is simulated. Using *method 1* described in the previous section, we can understand the dependency that χ_e has on the temporal envelope of the laser pulse.

In a similar manner to deriving eqn 2.13 for a Gaussian laser pulse in Chapter 2, one could determine the exact analytical form of $\langle\chi_e\rangle$ for our asymmetric intensity profile by integrating eqn 3.15, namely

$$\int_{-\infty}^{t} I(\beta, t)\ \mathrm{d}t$$

where,

$$I(\beta, t) = \exp\{-t^2/(2\tau_p^2)[1 + \beta t/(t^2 + \tau_p^2)^{0.5}]^{-1}\}$$

However, this integration is troublesome and cannot be performed using standard mathematical functions. This is because we are integrating a complicated variant of the Gaussian function which does not exist. However, this can be overcome by either using a numerical integration scheme or our numerical PIC code to simulate the asymmetric pulse and calculate the electron's χ_e as described in section 3.3.

If we assume that our laser temporal intensity envelope has a constant peak, then our simulations indicate that skewing the laser pulse encourages higher values of χ_e. Since we are arbitrarily modifying the laser intensity profile, the peak of the pulse is also displaced moving further toward the point at which the electrons enter the pulse. By applying laser pulse skewness, in effect, allowing the electrons to reach the peak of the intensity profile I_0 before the electrons lose significant energy to radiation reaction. This effect can be clearly observed in fig 3.13 which shows how the 1.5GeV electrons evolve in the collision with

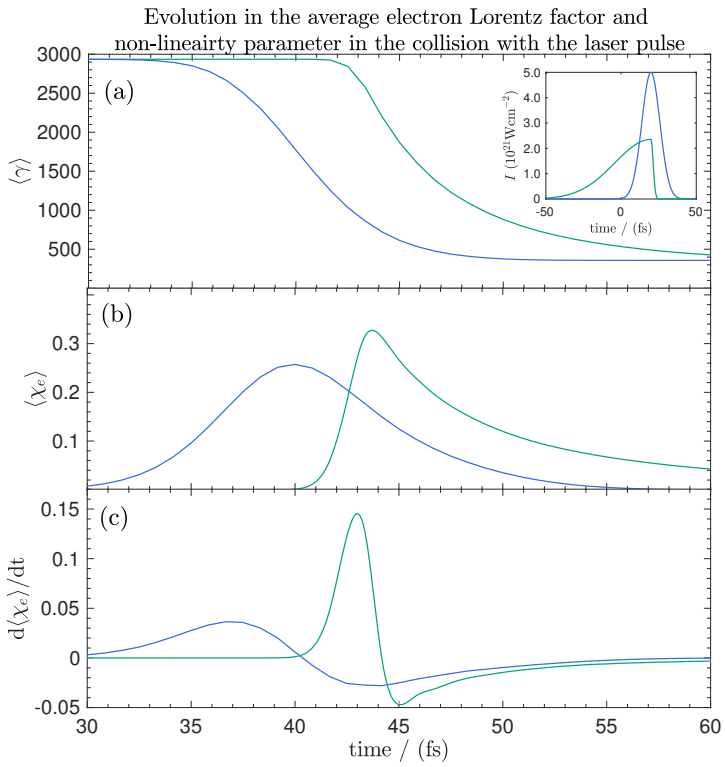

Figure 3.13: PIC code results using the quantum radiation reaction model. (a) The average electron's Lorentz factor $\langle\gamma\rangle$ and (b) electron's non-linearity parameter $\langle\chi_e\rangle$ and (c) derivatives using a $5\times10^{21}\mathrm{Wcm}^{-2}$ 40fs Gaussian (blue) and Skewed Gaussian (green) pulse. Inset: laser intensity spectrum for the respective temporal envelopes.

a short 40fs $5\times10^{21}\mathrm{Wcm}^{-2}$ Gaussian and skewed Gaussian envelope. The three subplots are the average electrons Lorentz factor $\gamma(t)$ (a), average χ_e (b) and corresponding derivative in time (c). The electrons in the skewed envelope loose energy at some time t' after the electrons begin to loose energy in the Gaussian pulse. This indeed changes the average χ_e of the electron bunch in the skewed Gaussian giving electrons with higher maximum χ_e. If however, the short Gaussian envelope had a faster rising leading edge, the envelope without a skew would have electrons with maximum χ_e. One can see in (c) that maximum χ_e, where the derivative passes through 0 is at 40fs for the Gaussian and approximately 45fs for the skewed Gaussian. Therefore, radiation reaction and energy loss through emission of hard photons is highly dependant on

the time the electrons travel in the pulse. This result is in agreement with our previous finding in fig 2.6, showing that higher initial energy electrons maintain a higher average χ_e.

The effect to consider is electron straggling or *quenching*, this effect in the laser pulse plays an important role in the number of electrons with a high non-linearity parameter. This phenomenon is a consequence of the probabilistic nature of the emission process, whereby electrons can travel through the laser pulse without emitting any or very little high-energy photons [72]. Therefore, observing straggling in a sufficient number of electrons may be advantageous in observing electrons with reasonably high values of χ_e. Particularly this effect could play an important role for those straggling electrons that reach the peak of the pulse without loss of energy to radiation reaction.

For instance, a $5 \times 10^{21}\mathrm{Wcm}^{-2}$ pulse colliding with a 1.5GeV electron-beam in theory could possibly have straggling electrons at the peak of the pulse with a $\chi_e \approx 0.6$. Although, the effect of straggling on the temporal envelope of the pulse has to our knowledge not been considered previously. We would expect the following to occur if a skew is added to the envelope. A faster rising leading edge of the pulse could improve the number of straggling electrons due to the shorter time in reaching the centre of the pulse as demonstrated in fig 3.13. However, with the reduction of the peak intensity, the number of high energy laser photons would be reduced and therefore produce lower pair yields. This curtailing of pair yields will be considered in section 3.4.3.

3.4.2 *Effect of skewing on the electron distributions*

The quantum model using the Monte-Carlo algorithm of radiation reaction incorporates the stochastic nature of the emission and the electrons trajectory after the collision with the laser pulse. Therefore, the distribution in the electron's non-linearity parameter χ_e, $f(\chi_e)$ allows one to determine how many electrons have lost significant energy, or those electrons which have radiated a higher number of photons and those which have not. The loss of energy of an electron with $\chi_e \gg 1$ goes from $0.44\chi_e$ to $1 - 4/(3\chi_e)$, therefore showing that at $\chi \geq 1$ the electron can lose a much higher fraction of its energy to radiation reaction. Clear differences are observed between the electron χ_e distributions as we compare a Gaussian temporal envelope and a pulse which has a noticeable asymmetry caused by a fast or slow rising leading edge of the laser pulse. In this section, we will determine the differences in the electron non-linearity parameter distributions for a Gaussian and skewed Gaussian envelope.

Consider the peak laser electric field as held constant such that E_0 does not reduce with non-zero values of the skew parameter β of the laser pulse, we observe a significant increase in the electron's χ_e demonstrated in fig. 3.14. Using the quantum model of radiation reaction, we have simulated a 1000 electron bunch with three electron-beam energies $\mathcal{E}_0$ for both skewed $\beta = -1$ and non-skewed Gaussian profiles $\beta = 0$. In all three initial electron-beam energies in fig. 3.14, a skewed Gaussian pulse produces electrons with higher average χ_e. If we consider the average electron energy loss for a 2.0GeV electron-beam for $\beta = 0$ and $\beta = -1$ respectively, we find the following: the average χ_e for a $2 \times 10^{21}\text{Wcm}^{-2}$ with peak electric field $E_0 = 8.6822 \times 10^{13}\text{Vm}^{-1}$ Gaussian pulse is $\langle \chi_e \rangle = 0.2785$, thus the Lorentz factor of these electrons is $\gamma = 2117$ with energy 1081MeV, (1.081GeV). Similarly, for the neg-

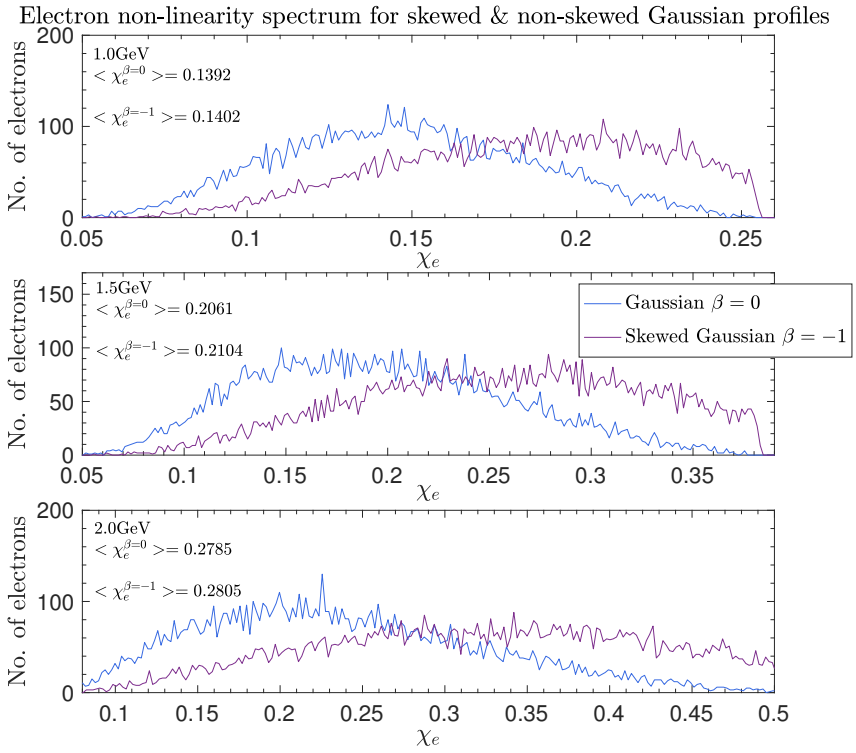

Figure 3.14: A constant peak: comparing the electron χ_e distribution for an electron bunch with different initial energies $\mathcal{E}_0$, namely (a) 1GeV (b) 1.5GeV and (c) 2.0GeV for both Gaussian $\beta = 0$ and negatively skewed Gaussian $\beta = -1$ by applying *method 2*.

atively skewed Gaussian $\langle \chi_e \rangle = 0.2805$, where $\gamma = 2132$ therefore an energy of 1089 (1.089GeV). The highest energy electrons are produced using a 2.0GeV electron-beam reaching a non-linearity parameter in excess of $\chi_e \sim 0.5$. Calculating the electron's energy for a $\chi_e > 0.5$, the Lorentz factor of these electrons is $\gamma = 3801$, thus an energy of 1.574GeV. Therefore, the few electrons at high χ_e have lost 40% of their initial energy to radiation reaction as $\chi_e \geq 0.1$.

Now consider the effect that experimentally skewing the temporal envelope gives a reduction in the peak intensity of the laser I_0 and the consequences this has on the electron χ_e distributions. The electron distribution in χ_e has been measured at the same instance in time as the electrons are at the center of the Gaussian pulse and at the leading rising edge of the skewed pulse, shown in fig 3.15. Comparing

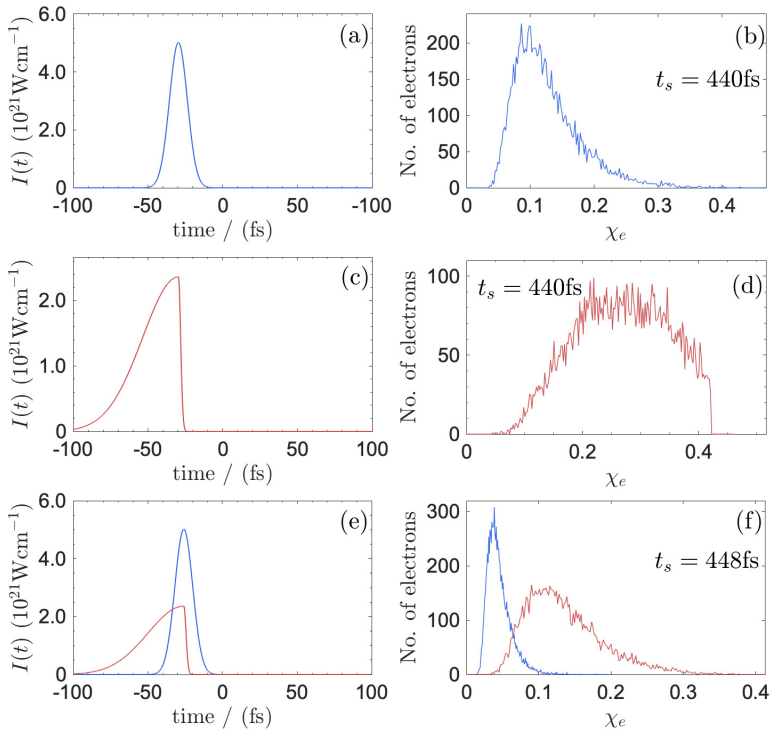

Figure 3.15: Comparing the distribution in the electron non-linearity parameter for negatively skewed and Gaussian temporal intensity envelops. (a)-(b) Gaussian envelope when the electron-beam is at the peak. (c)-(d) Skewed Gaussian envelope when the electron-beam is at the peak. (e)-(f) 8fs after the electrons reach the peak.

the distributions in (b) and (d), it can be observed that the average electron χ_e is significantly higher for the Gaussian which has a faster rise time, $\langle\chi_e\rangle \approx 0.25$ whereas it is $\langle\chi_e\rangle \approx 0.1$ without a skew. The sharp edge of the distribution in (d) shows the electrons that have not yet started to loose energy. We have also plotted the distributions for the two pulses in (f) which is measured 8fs after the collision with the skewed envelope and 8fs from the peak of the Gaussian pulse. This shows the electrons in the Gaussian pulse have lost considerable energy to photon emission as $\langle\chi_e\rangle < 0.1$. The χ_e distributions for the skewed envelope appears to still have a reasonably high average $\chi_e \approx 0.1$ and maximum $\chi_e \approx 0.3$.

As χ_e depends on both the Lorentz factor of the electrons $\gamma(t)$ and the external laser field, suggesting that the skewed envelope gives higher

maximum χ_e, the external field of the intensity envelope will be in competition with $\langle\gamma\rangle$ in the increase and probability of electron-positron pair production via Breit-Wheeler, shown in fig. 3.4.

3.4.3 *Enhancing electron-positron pair yields*

Our simulation results show an increase to the electron's non-linearity parameter if we apply a skew to the leading rising edge of the pulse. Previously, the dependency on pulse duration and pulse shape to enhance pairs have been considered by N. Neitz and A. Di Piazza [73], finding that a laser profile with a shorter pulse duration encourages the improvement of pair yields. Similar results performed by O. Oluk *et al* [74] also shows numerically that the pair number density monotonically decreases as the ratio of longer to fixed pulse lengths increases. We shall now determine the effect that skewing the laser pulse has on electron-positron pair yields from our QED-PIC simulations.

This has been achieved by measuring the number of positrons created after the collision of the pulse with the electron-beam. Following the skewing method outlined in *method 1*, a short 40fs Gaussian pulse is employed and a negatively skewed temporal envelope is simulated using a variety of different values of τ_r and τ_f provided in table 3.1. The number of pairs produced in which the edge of the laser pulse sharply increases are shown in fig 3.16 for a given scaled peak intensity $I_1 = \mathcal{R}I_0$.

$\mathcal{E}_0$ (GeV)	τ_r (fs)	τ_f (fs)	$\mathcal{R}I_0$ (10^{21}Wcm^{-2})	$N_\pm/N_e$
1.5	40	40	5.0	1.9554×10^{-5}
1.5	20	120	2.86	2.7637×10^{-6}
1.5	10	160	2.35	1.4944×10^{-6}

Table 3.1: Simulation results giving the number of electron-positron pair yields per electron after the collision of a 1.5GeV electron-beam with a 5×10^{21}Wcm^{-2} Gaussian and skewed Gaussian pulse.

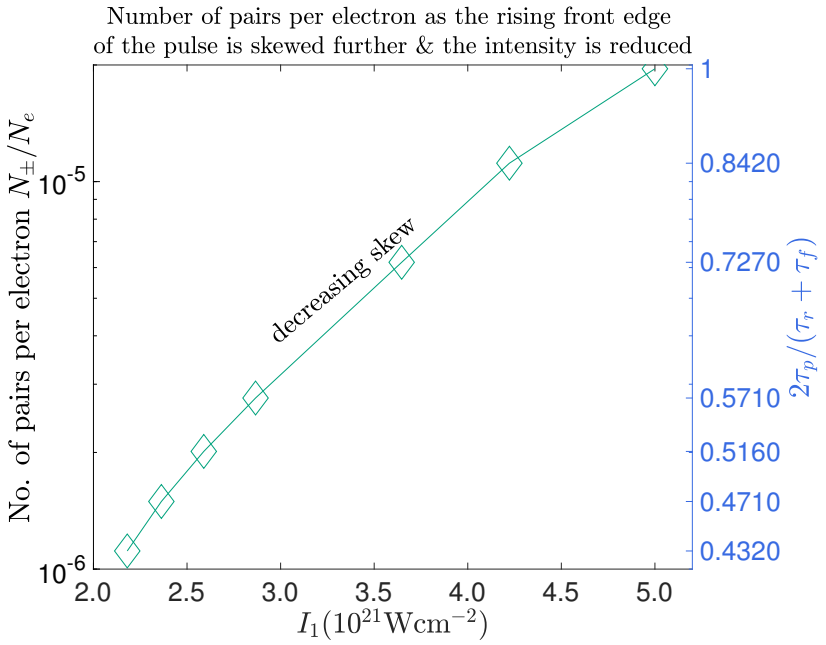

Figure 3.16: PIC code results showing the electron-positron pair yields per electron $N_\pm/N_e$ for initial peak intensity $I_0 = 5\times10^{21}\mathrm{Wcm}^{-2}$. As the rising edge becomes faster, the peak is reduced by $\mathcal{R}$ giving a new peak $I_1 = \mathcal{R}I_0$. The right-hand axis gives the amount that the intensity spectrum is reduced by.

We use *method 1* to simulate using a $\tau_r = 10$fs at the leading edge and a longer 160fs as the falling time to produce the skew. We discover that a pulse which has a Gaussian envelope gives pair yields of $N_\pm/N_e \approx 1.9554\times10^{-5}$ while a significant skew reduces the yields by an order of magnitude to 1.4944×10^{-6}. This corresponds to a scaling of the intensity by as much as 53% to $2.35\times10^{21}\mathrm{Wcm}^{-2}$. This indicates that pair yields are curtailed as the sharp rise of a skewed Gaussian pulse is increased, dependent on the drop in the peak intensity, I_1. Shown in fig 3.17 is the convergence testing performed on the number of pair yields as the simulation grid and particles number is increased. Considering the simulation grid first, the convergence testing shows that the Gaussian gives a mean of $\langle N_\pm/N_e\rangle \approx 1.67\times10^{-5}$ with a standard deviation of $\sigma \approx 6.43\times10^{-6}$. The skewed Gaussian has a mean $\langle N_\pm/N_e\rangle \approx 2.14\times10^{-6}$ and $\sigma \approx 2.38\times10^{-6}$, an order of magnitude lower than the Gaussian envelope. These tests show that convergence

is improved on as the grid size increases. Although convergence at a given value has not been achieved in these tests, it does show that the results do not deviate from the 10^{-5} order and are consistent with the overall result in number of pairs between the two envelopes. Namely, the skewed Gaussian produces a lower order of pairs per electron than the Gaussian envelope. The convergence testing as the number of macro particles increases is fluctuating but does increase with a higher number of particles. The average number of pairs is $\langle N_{\pm}/N_e \rangle \approx 1.7 \times 10^{-5}$ with standard deviation $\sigma \approx 2.3 \times 10^{-6}$. We find that the skewed Gaussian gives $\langle N_{\pm}/N_e \rangle \approx 1.4 \times 10^{-6}$ and a $\sigma \approx 7.1 \times 10^{-7}$. This demonstrates that the convergence using the number of particles is more sensitive to statistical noise, however by determining the mean value we can see that baseline simulation parameters (red point in fig 3.17) is a reasonable parameter set to use.

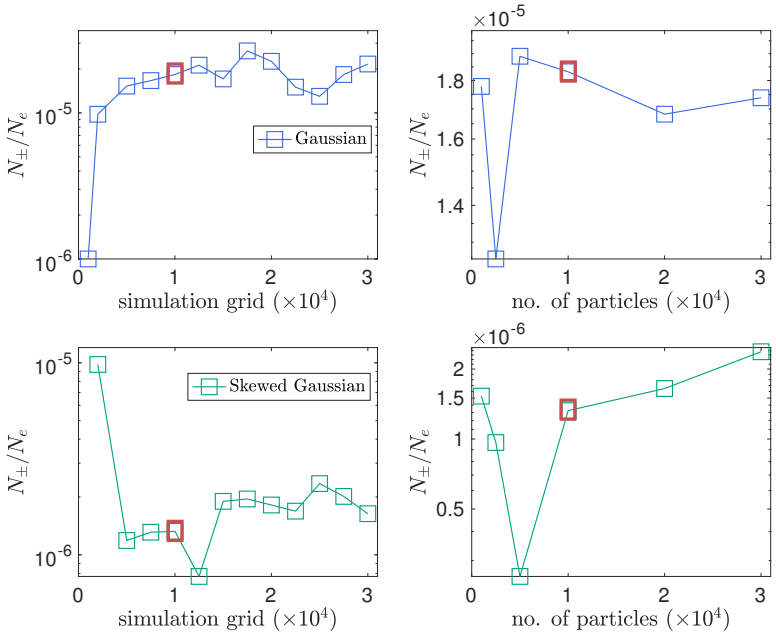

Figure 3.17: Convergence testing on the number of e^-e^+ pairs per electron produced for Gaussian and skewed Gaussian envelopes as the simulation global grid and particle size is increased. The red point indicates the baseline parameters used in this work.

Further simulations were performed by varying the intensity of the laser and measuring the pair yields per electron $N_{\pm}/N_e$ at the end of the simulation. Provided in fig 3.18, for intensities from 2×10^{21} to $20 \times 10^{21}\text{Wcm}^{-2}$, it is shown that pair yields are significantly curtailed at lower intensities for the skewed Gaussian envelope $N_{\pm}/N_e \sim 10^{-10}$ and increase by a factor ~ 100 with a short compressed Gaussian envelope. The number of pairs produced for both Gaussian and skewed Gaussian envelopes at higher intensities begin to approach each other. This may be due to numerical error in the PIC code rather than a physical effect at higher intensities.

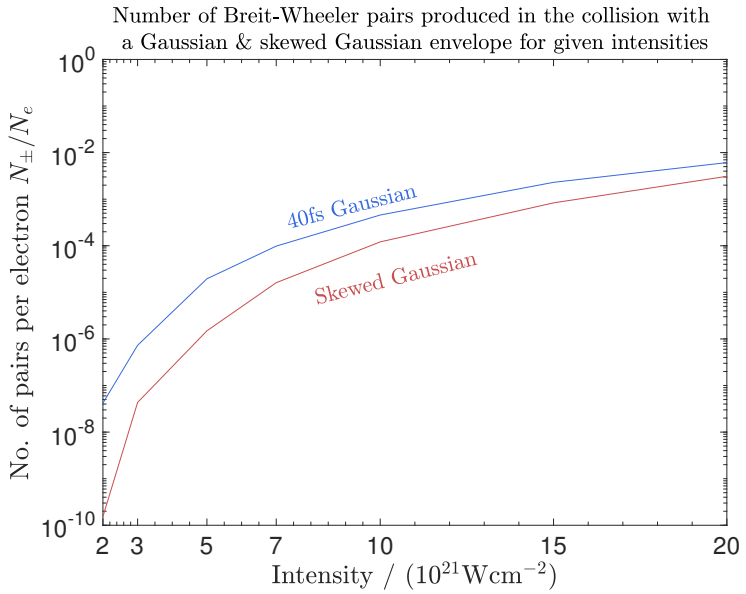

Figure 3.18: Comparing the electron-positron pair yields per electron $N_{\pm}/N_e$ for a Gaussian and skewed Gaussian envelope. The laser wavelength is 1μm and initial electron-beam energy $\mathcal{E}_0$ is 1.5GeV.

These results show the high dependency on laser parameters, specifically the peak intensity in enhancing electron-positron pair yields. Although the energy in the two pulses are equal, the higher pair yield in the Gaussian envelope is due to the higher peak intensity (higher energy laser photons) of the external laser field. We will now consider experimental constraints and simulate realistic temporal envelopes to determine compare the results found in this section.

3.5 EXPERIMENTAL CONSIDERATIONS

3.5.1 *In optically skewing the laser pulse envelope*

The parameters in these simulation results are available with current PW lasers, as we must also consider the validity of these results against experimental and physical constraints. Since active mode-locking, at moderate dispersion, the shape of a typical laser pulse is approximately Gaussian with more complicated shapes posing a challenging optical feat. The pulse shape used in the Leemans experiments [30], in order to modify the shape, changed the laser frequency spectrum by detuning the compressor of the pulse in the compression stage of Chirped-pulse-amplification (CPA). The detuning using an optical grating offsets the third order phase [75], therefore producing a fast rising edge of the pulse. Although insightful theoretically, the temporal asymmetry of the laser pulses in [28] appear unphysical with a large unbounded peak and do not account for experimentally tested pulse shapes and the effect that the reduction in the peak laser intensity I_0 has on the number of BW e^-e^+ pairs produced.

Now we will consider experimental pulse shapes that can be produced through optical modification. The temporal envelopes in fig 3.19 are realistic laser pulses[1]. The Gaussian pulse in (a) of fig 3.19 is a compressed $1.5 \times 10^{22}\text{Wcm}^{-2}$ 50fs pulse, an asymmetric pulse in (b) is the result of modifying the pulse phase and (c) is a LWFA simulation where a pulse is driven through a 20mm plasma with electron density $n_e = 2 \times 10^{18}\text{cm}^{-3}$. Inspection of the respective pulses, we observe that (c) has the highest peak E_0 followed by (a) and lastly (b) shown in table 3.2. However in (c), the peak E_0 of this pulse drops immediately. The asymmetric pulse in (b) has the lowest peak electric field and therefore

1 Temporal electric field envelopes provided by M. J. V. Streeter, Blackett Laboratory, Imperial College London, London SW7 2AZ, UK

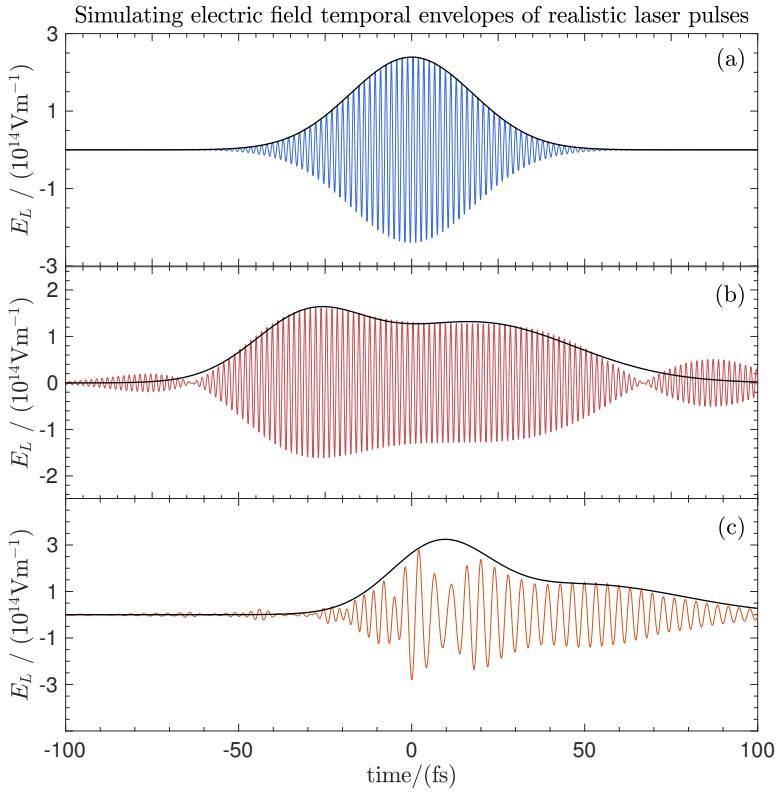

Figure 3.19: Comparing experimental and theoretical peak electric field of the temporal laser pulse. (a) a 50fs Gaussian laser pulse with peak $E_0 = 2.3931 \times 10^{14}\text{Vm}^{-1}$. (b) Peak laser electric field for a skewed Gaussian pulse with $E_0 = 1.6104 \times 10^{14}\text{Vm}^{-1}$ (c) skewed pulse produced from a LWFA simulation $E_0 = 2.7919 \times 10^{14}\text{Vm}^{-1}$.

lowest peak intensity I_0. The short compressed Gaussian pulse has both a high E_0 and over a longer duration.

By adding two Gaussian functions $\zeta(t) = \phi(t) + \psi(t)$, where $\phi(t)$ is an envelope with peak E_0, pulse duration τ_p and $\psi(t)$ has a different peak and duration, E_0' and τ_p' respectively. We have fitted these pulse shapes shown in fig 3.19 accordingly. As can be seen, these fits are within good approximations to the pulse shapes and therefore can be used to simulate realistic pulse shapes in our QED-PIC. The fit in (c) of fig 3.19 however may be an overestimate of the true pulse shape due to the varying laser amplitude produced by the wakefield. The results of

Pulse shape	E_0 $(10^{14}\mathrm{Vm}^{-1})$	$N_\pm / N_e$
50fs Gaussian	2.3931	1.90×10^{-2}
Asymmetric Gaussian	1.6104	8.8575×10^{-5}
LWFA	2.7919	7.90×10^{-2}

Table 3.2: Simulating realistic pulse shapes to determine pair yields for a 50fs compressed Gaussian, a Gaussian with a negative chirp and a temporal envelope produced from a LWFA simulation in FBPIC.

these simulations are shown in table 3.2, as expected the pair yields per electron is maximum at 7.90×10^{-2} for the pulse generated in by the LWFA, secondly is the compressed Gaussian pulse at 1.90×10^{-2} and lastly with the lowest produced pairs is the asymmetric Gaussian with 8.8575×10^{-5}. Indeed, these results are consistent to the reduction to the number of pairs produced with temporal envelopes in our PIC code provided in table 3.1. The three orders of magnitude difference in pair yields for the two tables using the Gaussian is a consequence of simulating a higher initial peak electric field, namely $2.3931 \times 10^{14}\mathrm{Vm}^{-1}$.

3.5.2 *In plasma optics: employing a plasma target*

Plasma-based focusing optics have been suggested to increase the laser intensity by an order of magnitude [76] as well as curved shaped plasma targets [77] to study QED effects. As we discovered in the previous section, a pulse generated via laser wakefield acceleration had a high electric field peak E_0 and higher pair yield over the asymmetric pulse. Driving the laser pulse into a plasma mirror may be the optimum way in order to create the fast rise at the front of the laser pulse as it is reflected back on itself without reducing the peak intensity I_0. The principle of the plasma mirror is that once the electron density n_e of the plasma exceeds the critical density n_c in which case the plasma is overdense, reflection of the incoming laser pulse is achieved producing a chirp [78]. Similar plasma mirrors on the Gemini system at Rutherford Appleton Laboratory, STFC have been used previously [79].

The method of pulse shaping is in relativistic self-phase-modulation (SPM) in which photons in a plasma at the leading front edge decelerate and cause the fast rising chirp [80]. The refractive index η of the pulse varies longitudinally as a function of time in the plasma ensuing a shift in the phase and broadening of the frequency spectrum. The pulse is red shifted at the front of the pulse as η increases causing a sharp rise in the peak intensity. The frequency at the rear side of the pulse is blue shifted attributed to a decrease in η, it is this change in η and the group velocity v_g that causes an asymmetry in the temporal envelope.

Our PIC code model described in *method 1* in section 3.3.1 is not an unrealistic scenario in modeling the temporal asymmetry on the pulse since pulse duration shortening in a plasma by modulation [81] and compression [82] can be achieved and is experimentally feasible. However, the main challenge is in modifying the envelope on an ultrashort

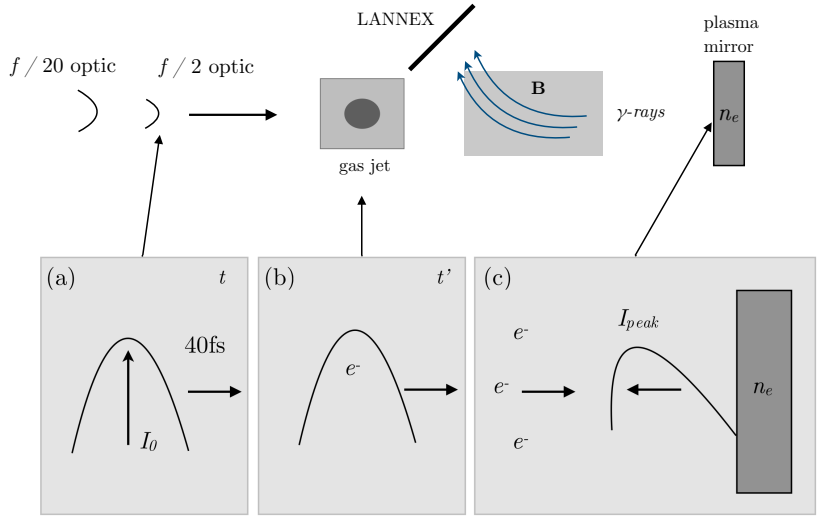

Figure 3.20: Proposed experimental set up of a plasma optical scheme. (a) an $f/2$ laser is driven towards a plasma mirror at time t. (b) Some delayed time t' after the first laser shot, a second $f/20$ optic is used as a laser wakefield to accelerate the electrons from a helium gas jet to GeV energy in the direction of the plasma mirror separated by a distance zm. (c) the leading edge of the short 40fs 10^{21}Wcm^{-2} $f/2$ pulse is reflected back on itself where the peak of the laser I_{peak} reverses creating an increase in peak intensity as the electrons enter the reflected skewed pulse.

femto-second timescale as longer nanosecond temporal pulse shaping has been demonstrated [83].

The proposed experimental scheme is illustrated in fig. 3.20 which shows an $f/2$ short 40fs pulse optic incident at time t on a plasma mirror with electron density n_e. A second $f/20$ laser propagates through a pin hole of the $f/2$ optic to reach the interaction area. This laser pulse is used as the wakefield to accelerate an electron bunch from a supersonic helium gas jet to ∼GeV energies in the direction of the mirror. The mirror reflects the first pulse creating the fast rise at the leading edge and propagates counter to the electron-beam. Further 2D plasma PIC code simulations could be performed in order to further understand the challenges and feasibility of this scheme.

4

CONCLUSION

The purpose of this thesis has been to understand if the electron's non-linearity parameter is maximised in a Gaussian laser pulse with a fast rising edge. As the electrons reach the peak of the laser intensity temporal envelope having lost less energy to quantum radiation reaction, electron-positron pair enhancement could be possible.

In Chapter 2, our analytical model for $\langle \chi_e \rangle$ derived *ab initio* found that maximum χ_e is not at the peak and depends on the initial energy $\mathcal{E}_0$ of the electrons before entering the pulse. We further discovered that sensitivity in the pulse duration can increase χ_e finding a factor of two increase in going from a long 150fs pulse to short 30fs pulse durations, corresponding to a higher strength parameter a_0.

In Chapter 3 we simulated QED effects at $a_0 \gg 1$, showing that the average behavior of the electrons χ_e in a Gaussian pulse is identical to average γ, discovered by C. P. Ridgers *et al* [64], using the classical, modified-classical and quantum RR models. Namely, a broadening of the electrons χ_e distribution for stochastic quantum RR and a narrowing in both classical and modified-classical models as the electrons emit radiation.

We proposed two methodologies to model asymmetric Gaussian temporal envelopes in a QED-PIC code. One which uses the symmetry of a Gaussian pulse to change the pulse duration on either side of the peak. A second method which gives the explicit analytical form of the intensity profile with a skew parameter β, approximated from the Leemans experiment [30].

Contrary to previous PIC simulation results in C. Hojbota *et al* [28], we find that a combination of maximum peak intensity I_0 and a fast rising edge at the front of a skewed Gaussian pulse is unattainable. The pulses used in these simulations have an unphysical shape in which the peak intensity is unbounded. We have shown, by correcting the peak intensity with a scaling factor ($I_1 = \mathcal{R}I_0$), a negatively skewed $5 \times 10^{21}\text{Wcm}^{-2}$ Gaussian pulse in the head-on collision with 1.5GeV electrons produces 1.5×10^{-6} BW electron-positron pairs. Simulating identical parameters and keeping the energy in the two pulses conserved but instead with an unmodified compressed 40fs Gaussian pulse, the number of pairs produced is enhanced to 2.0×10^{-5}, a factor of ~ 10 improvement. Comparing with temporal envelopes from realistic pulses of a 50fs $1.5 \times 10^{22}\text{Wcm}^{-2}$ Gaussian and skewed Gaussian by phase offsetting, pair yields are 1.9×10^{-2} (Gaussian), 8.9×10^{-5} (skewed Gaussian) and 7.9×10^{-2} (pulse from LWFA) respectively.

In summary, a Gaussian intensity temporal envelope with a fast rising leading edge is *not* the optimum pulse shape to enhance observation of QED effects. Optimum electron-positron pair enhancement is achieved with a short compressed Gaussian pulse. A plasma optics scheme employing a plasma mirror to reflect the pulse back on itself, creating a fast rising edge, while maximising the peak intensity I_0 has been considered. As optically modifying the pulse produces an undesirable reduction to the peak intensity, a novel scheme which introduces a plasma may be a future route to enhance pair production at next-generation laser facilities.

4.1 OUTLOOK

The recent signatures of quantum radiation reaction demonstrates that current optical laser systems are moving closer towards experimental probing of quantum effects observed at $a_0 \gg 1$. Simulating laser - electron beam collisions that employ numerical methods such as a PIC code are invaluable tools. However, in the case of modifying the temporal envelope of the pulse optically or with the LWFA simulation, comparison to real experiment is of fundamental importance.

An analytical form for N_+, the number of positrons produced from an electron-beam has been derived previously by T. G. Blackburn *et al* [52]. This result could be compared to the PIC code results realised here by deriving N_+ for a laser pulse intensity profile with a skewed temporal envelope. This would provide a more rigorous analytical description of pair production for a skewed Gaussian pulse.

Furthermore, the analytical form of both eqn 2.11 and 2.13 assume $g(\chi_e) = 1$, failing to include quantum corrections to the synchrotron emission. Deriving a modified-classical version of these two equations would yield accurate results on the electrons evolution in a Gaussian envelope.

While it has been shown that adding a skew to the laser temporal envelope reduces the pair yields, our plasma scheme to a create fast rising envelope while maintaining I_0 would need to be tested using a suitable particle-in-cell code.

A

APPENDIX

A.1 ENERGY IN THE SUPERGAUSSIAN PULSE

Starting with the supergaussian of order n temporal envelope with peak field E_n and pulse duration τ_p

$$E(t) = E_n e^{-(t/\tau_p)^n}$$

The energy in the pulse is therefore given by integrating over the square of $E(t)$

$$\mathcal{E} \propto \int_{-\infty}^{\infty} E^2(t)\ dt$$

Consider integrating for $t > 0$

$$\begin{aligned} \mathcal{E} \propto \int_0^{\infty} E_n^2 e^{-2(t/\tau_p)^n}\ dt &= \int_0^{\infty} E_n^2 e^{-(2^{(1/n)}t/\tau_p)^n}\ dt \\ &= \int_0^{\infty} E_n^2 e^{-(t/\tau_p')^n}\ dt \end{aligned} \tag{A.1}$$

where the substitution $\tau_p' = \tau_p/2^{1/n}$ has been made and changing variables by letting $x = (t/\tau_p')^n$ with derivative given by

$$dx = \frac{nt^{n-1}}{\tau_p^{`n}} dt$$

Now changing variables by substituting $t = \tau_p' x^{1/n}$

$$dx = \frac{n}{\tau_p'} x^{1-1/n} dt$$

and therefore $dt = (\tau_p/n)x^{1/n-1}dx$ can be substituted into A.1

$$\mathcal{E} \propto \frac{E_n^2\tau_p'}{n}\int_0^\infty x^{(1/n-1)}e^{-x}\,dx = \frac{E_n^2\tau_p'}{n}\Gamma(1/n) \tag{A.2}$$

Since we know the energy in a Gaussian ($n = 2$) pulse, we may equate this with the energy in the n-th order as we wish the two energies to be equal $\mathcal{E}_2 = \mathcal{E}_n$

$$\frac{E_n^2\tau_p}{2^{1/n}n}\Gamma(1/n) = \frac{E_0^2\tau_p'\sqrt{\pi}}{2^{3/2}}$$

Simplifying and rearranging gives the result

$$\left(\frac{E_n}{E_0}\right)^2 = \frac{I_n}{I_0} = \frac{2^{1/n}n\sqrt{\pi}}{2^{3/2}\Gamma(1/n)}$$

A.2 SIMULATION RESULTS FROM QED-PIC CODE

Below are the PIC code results showing the number of electron-positron pairs per electron used to produce fig 3.18.

$\mathcal{E}_0$ (GeV)	I_0 (10^{21}Wcm^{-2})	$N_\pm / N_e$
1.5	1.0	0
1.5	2.0	4.20×10^{-8}
1.5	3.0	7.30×10^{-7}
1.5	5.0	1.96×10^{-5}
1.5	7.0	9.83×10^{-5}
1.5	10.0	4.57×10^{-4}
1.5	15.0	2.3×10^{-3}
1.5	20.0	6.1×10^{-3}

Table A.1: PIC code simulation results giving the number of electron-positron pair yields per electron for a given *Gaussian* laser intensity.

$\mathcal{E}_0$ (GeV)	I_0 (10^{21}Wcm^{-2})	$N_\pm / N_e$
1.5	1.0	0
1.5	2.0	1.54×10^{-10}
1.5	3.0	4.33×10^{-8}
1.5	5.0	1.49×10^{-6}
1.5	7.0	1.61×10^{-5}
1.5	10.0	1.21×10^{-4}
1.5	15.0	8.33×10^{-4}
1.5	20.0	3.1×10^{-3}

Table A.2: PIC code simulation results giving the number of electron-positron pair yields per electron for a given *Skewed Gaussian* laser intensity.

[1] Vulcan 2020. URL: https://www.clf.stfc.ac.uk/Pages/Vulcan-2020.aspx.

[2] Exteme Light Infrastructure (ELI). URL: https://eli-laser.eu.

[3] Apollon. URL: https://aries.web.cern.ch/content/apollon.

[4] T. Grismayer et al. "Laser absorption via quantum electrodynamics cascades in counter propagating laser pulses." Phys. Plasmas **23**.056706 (2016).

[5] A. V. Bashinov and A. V. Kim. "On the electrodynamic model of ultra- relativistic laser-plasma interactions caused by radiation reaction effects." Phys. Plasmas. **20(11)**.113111 (2013).

[6] A. D. Piazza et al. "Investigation of classical radiation reaction with aligned crystals." Phys. Lett. B **765**.1 (2016).

[7] M. Vranic et al. "QED vs. classical radiation reaction in the transition regime." API Con **1777**.050006 (2016).

[8] N. Neitz et al. "Novel aspects of radiation reaction in the classical and the quantum regime." J. Phys. Con **497**.012015 (2014).

[9] J. M. Cole et al. "Experimental Evidence of Radiation Reaction in the Collision of a High-Intensity Laser Pulse with a Laser-Wakefield Accelerated Electron Beam." Phys. Rev. X **8**.011020 (2018).

[10] N. Tobias et al. "Experimental evidence of quantum radiation reaction in aligned crystals." Nature Communications **9**.795 (2018).

[11] K. Poder et al. "Experimental Signatures of the Quantum Nature of Radiation Reaction in the Field of an Ultraintense Laser." Phys. Rev. X **8**.031004 (2018).

[12] J. R. Marques et al. "Temporal and Spatial Measurements of the Electron Density Perturbation Produced in the Wake of an Ultrashort Laser Pulse." Phys. Rev. Lett. **76**.19 (1969).

[13] D. Gauthier et al. "Chirped pulse amplification in an extreme-ultraviolet free-electron laser." Nature. Com. **7**.13688 (2016).

[14] D. Strickland and G. Mourou. "Compression of amplified chirped optical pulses." Opt. Comm. **56**.3 (1985).

[15] P. Gibbon. "Short Pulse Laser Interactions With Matter: An Introduction". Imperial College Press, (2005).

[16] S.-W. Bahk et al. “Generation and characterization of the highest laser intensities.” Opt. Lett. **29**.2837 (2004).

[17] J. Schwinger. “On Gauge Invariance and Vacuum Polarization.” Phys. Rev. **82**.5 (1951).

[18] C Bula et al. “Observation of Nonlinear Effects in Compton Scattering.” Phys. Rev. Lett **76**.17 (1996).

[19] D. L. Burke et al. “Positron Production in Multiphoton Light-by-Light Scattering.” Phys. Rev. Lett. **79**.9 (1997).

[20] I. C. E. Turcu et al. “Strong field physics and QED experiments with ELI-NP 2x10PW laser beams.” AIP Con. Pro. **1645**.416 (2015).

[21] G. Sarri et al. “Generation of neutral and high-density electron-positron pair plasmas in the laboratory.” Nature Comms **6**.6747 (2015).

[22] A. K. Harding and D. Lai. “Physics of strongly magnetized neutron stars.” Rep. Prog. Phys. **69**.2631 (2006).

[23] W. Luo et al. “Enhanced electron-positron pair production by two obliquely incident lasers interacting with a solid target.” Plas. Phys. Con. Fus. **60**.095006 (2018).

[24] X. L. Zhu et al. “Dense GeV electron?positron pairs generated by lasers in near-critical-density plasmas.” Nature Comms **7**.13686 (2016).

[25] N. Abdukerium et al. “Enhanced electron-positron pair production by frequency chirping in one- and two-color laser pulse fields.” Chin. Phys. B **26**.2 (2017).

[26] M. Lobet et al. “Generation of high-energy electron-positron pairs in the collision of a laser-accelerated electron beam with a multipetawatt laser.” Phys. Rev. Acccelerators & Beams. **20**.043401 (2017).

[27] H. X. Chang et al. “Generation of overdense and high-energy electron-positron-pair plasmas by irradiation of a thin foil with two ultraintense lasers.” Phys. Rev. E. **92**.053107 (2015).

[28] C. I. Hojbota et al. “Effect of the temporal laser pulse asymmetry on pair production processes during intense laser-electron scattering.” Plas. Phys. Con. Fus. **60**.064004 (2018).

[29] I. A. Aleksandrov, G. Plunien, and V. M. Shabaev. “Pulse shape effects on the electron-positron pair production in strong laser fields.” Phys. Rev. D. **95**.056013 (2017).

[30] W. P. Leemans et al. “Electron-Yield Enhancement in a Laser-Wakefield Accelerator Driven by Asymmetric Laser Pulses.” Phys. Rev. Lett. **89**.17 (2002).

[31] I. A. Andriyash et al. “Laser-plasma interactions with a Fourier-Bessel particle-in-cell method.” Phys. Plasmas. **23**.033110 (2016).

[32] D. J. Griffiths. "Introduction to Electrodynamics". Prentice Hall, (1999).

[33] D. J. Jackson. "Classical Electrodynamics". John Wiley & Sons Inc, (1998).

[34] A. D. Piazza. “Exact Solution of the Landau-Lifshitz Equation in a Plane Wave.” Lett. Math. Phys. **83**.305 (2008).

[35] S. V. Bulanov et al. “Lorentz-Abraham-Dirac versus Landau-Lifshitz radiation friction force in the ultrarelativistic electron interaction with electromagnetic wave (exact solutions).” Phys. Rev. E. **84**.056605 (2011).

[36] T. Erber. “High Energy electromagnetic conversion processes in intense magnetic fields.” Rev. Mod. Phys **5** (1966).

[37] V. N. Baier, V. M. Katkov, and V. M. Strakhovenko. "Electromagnetic Processes at High Energies in Oriented Single Crystals." World Scientific, (1998).

[38] C. P. Ridgers et al. “Dense electron-positron plasmas and bursts of gamma-rays from laser-generated quantum electrodynamic plasmas.” Phys. Plasmas. **20**.056701 (2013).

[39] G. Brodin et al. “Quantum-Electrodynamical Photon Splitting in Magnetized Nonlinear Pair Plasmas.” Phys. Rev. Lett **98**.125001 (2007).

[40] J. S. Heyl and L. Hernquist. “A QED Model for the Origin of Bursts from Soft Gamma Repaters and Anomalous X-ray Pulsars.” The Astrophysical Journal **618**.463-473 (2005).

[41] M. Tavani et al. “Discovery of Powerful Gamma- Ray Flares from the Crab Nebula.” Science. **331**.736 (2017).

[42] I. Caiazzo and J. Hayl. “Probing Black Hole Magnetic Fields with QED.” Galaxies. **57**.6(2) (2018).

[43] L. D. Landau and E. M. Liftshitz. "The Classical Theory of Fields". Elsevier, Oxford, (1975).

[44] W. H. Furry. "On Bound States and Scattering in Positron Theory." Phys. Rev **81**.1 (1951).

[45] S. S. Bulanov et al. "Schwinger Limit Attainability with Extreme Power Lasers." Phys. Rev. Lett. **105**.220407 (2010).

[46] S. Kneip et al. "Near-GeV Acceleration of Electrons by a Nonlinear Plasma Wave Driven by a Self-Guided Laser Pulse." Phys. Rev. Lett **103**.035002 (2009).

[47] H. T. Kim et al. "Enhancement of Electron Energy to Multi-GeV Regime by a Dual-Stage Laser-Wakefield Accelerator Pumped by Petawatt Laser Pulses." Phys. Rev. Lett **111**.165002 (2013).

[48] Mangles S. P. D. et al. "Laser-Wakefield Acceleration of Monoenergetic Electron Beams in the First Plasma-Wave Period." Phys. Rev. Lett. **96**.215001 (2006).

[49] N. V. Elkina et al. "Qed cascades induced by circularly polarized laser fields." Phys. Rev. ST Accel. Beams. **14**.054401 (2011).

[50] M. Vranic and others. "Quantum radiation reaction in head-on laser-electron beam interaction." New. J. Phys. **18**.073035 (2016).

[51] A. R. Bell and J. G. Kirk. "Possibility of Prolific Pair Production with High-Power Lasers." Phys. Rev. Lett. **101**.200403 (2008).

[52] T. G. Blackburn et al. "Scaling laws for positron production in laser - electron-beam collisions." Phys. Rev. A **96**.022128 (2017).

[53] N. Abdukerim, Z. L. Li, and B. Xie. "Effects of laser pulse shape and carrier envelope phase on pair production." Phys. Lett. B. **726**.820-826 (2013).

[54] Laser 4 Aton: 10 PW, 2kJ. URL: https://www.eli-beams.eu/en/facility/lasers/laser-4-10-pw-2-kj/.

[55] C. N. Harvey et al. "Quantum Quenching of Radiation Losses in Short Laser Pulses." Phys. Rev. Lett. **118**.105004 (2017).

[56] T. G. Blackburn, A. Ilderton, M. Marklund, and C. P. Ridgers. "Reaching supercritical field strengths with intense lasers." arXiv preprint **arXiv**.1808.03730 (2018).

[57] J. A. Gaunt. "Continuous Absorption." Philosophical Transactions of the Royal Society of London. Series A, Containing Papers of a Mathematical or Physical Character **229** (1930).

[58] K. K. Ansersen. "Experimental investigations of synchrotron radiation at the onset of the quantum regime." Phys. Rev. D. **86**.072001 (2012).

[59] A. A. Sokolov and I. M. Ternoc. "Synchrotron Radiation". Akademie-Verlag, Berlin, (1968).

[60] J. Schwinger. “The quantum correction in the radiation by energetic electrons.” Proc. Nat. Acad. Sci. **40**.2 (1954).

[61] V. N. Baier, V. M. Katkos, and V. M. Strakhovenko. “Quasi-classical theory of radiation and pair creation in crystals at high energy.” Rad. Eff. **527**.122-123 (1991).

[62] V. I. Ritus. “Quantum Effects of the Interaction of Elementary Particles with an Intense Electromagnetic Field.” J. Sov. Laser Res. **6**.497 (1985).

[63] J. G. Kirk, A. R. Bell, and I. Arka. “Pair production in counter-propagating laser beams.” Plas. Phys. Con. Fus. **51**.085008 (2009).

[64] C. P. Ridgers et al. “Signatures of quantum effects on radiation reaction in laser – electron-beam collisions.” J. Plasma. Phys **83**.715830502 (2017).

[65] G. Breit and J. A. Wheeler. “Collision of Two Light Quanta.” Phys. Rev. **46** (1934).

[66] T. D. Arber et al. “Contemporary particle-in-cell approach to laser-plasma modelling.” Plas. Phys. Con. Fus. **57**.113001 (2015).

[67] M. Vranic et al. “Classical radiation reaction in particle-in-cell simulations.” Com. Phys. Comm. **204**.141-151 (2016).

[68] C. P. Ridgers et al. “Modelling Gamma Ray Emission and Pair Production in High-Intensity Laser-Matter Interactions.” J. Comp. Phys. **260**.273 (2014).

[69] T. G. Blackburn et al. “Quantum Radiation Reaction in Laser-Electron-Beam Collisions.” Phys. Rev. Lett. **112**.015001 (2014).

[70] I. V. Sokolov et al. “Pair Creation in QED-strong Pulsed Laser Fields Interacting with Electron Beams.” Phys. Rev. Lett. **105**. 195005 (2010).

[71] W. P. Leeman et al. “Electron-Yield Enhancement in a Laser-Wakefield Accelerator Driven by Asymmetric Laser Pulses.” Phys. Rev. Lett. **89**.17 (2002).

[72] C. S. Shen and D. White. “Energy straggling and radiation reaction for magnetic bremsstrahlung.” Phys. Rev. Lett **28**.455 (1972).

[73] N. Neitz and A. Di. Piazza. “Electron-beam dynamics in a strong laser field including quantum radiation reaction.” Phys. Rev. A. **90**.022102 (2014).

[74] O. Oluk et al. “Electron-positron pair production in a strong asymmetric laser electric field.” Front. Phys. **9**.2 (2014).

[75] C. S. Tóth et al. “Tuning of laser pulse shapes in grating-based compressors for optimal electron acceleration in plasmas.” Opt Lett. **28**.19 (2003).

[76] J. Fuchs et al. “Plasma devices for focusing extreme light pulses.” Eur. Phys. J. Spec. Top. **223**.1169 (2014).

[77] A. A. Gonoskov et al. “Ultrarelativistic nanoplasmonics as a route towards extreme-intensity attosecond pulses.” Phys. Rev. E. **84**.046403 (2011).

[78] G. Doumy et al. “Complete characterization of a plasma mirror for the production of high-contrast ultraintense laser pulses.” Phys. Rev. E. **69**.026402 (2004).

[79] Astra Gemini compact plasma mirror system. URL: https://www.clf.stfc.ac.uk/Pages/ar08-09_s7_astra-gemini-compact.pdf.

[80] D. F. Gordon et al. “Asymmetric Self-Phase Modulation and Compression of Short Laser Pulses in Plasma Channels.” Phys. Rev. Lett. **90**.21 (2003).

[81] J. Faure et al. “Observation of Laser-Pulse Shortening in Nonlinear Plasma Waves.” Phys. Rev. Lett **95**.205003 (2005).

[82] J. Schreiber et al. “Complete Temporal Characterization of Asymmetric Pulse Compression in a Laser Wakefield.” Phys. Rev. Lett. **105**.235003 (2010).

[83] P. Oliveira et al. “Control of temporal shape of nanosecond long lasers using feedback loops.” Opt. Express **27**.6607-6617 (2019).